Cloud Structure on Venus with VIRTIS

J. K. Barstow

September 28, 2009

First Year Report

Lady Margaret Hall

Atmospheric, Oceanic and Planetary Physics, University of Oxford

$\sim$ 12500 words

Abstract

Near-infrared spectra from the Visible and Infrared Thermal Imaging Spectrometer (VIRTIS) on Venus Express provide the opportunity for investigating and constraining a wide range of atmospheric parameters for Venus. The aim of this work is to exploit the wealth of data available from Venus Express to better understand the behaviour of the Venusian clouds, which are known to play a significant role in the radiative balance of the planet. Initial work comparing forward models of the 2.3 μm window region (Allen & Crawford 1984) with VIRTISM-IR data has resulted in a better 4-mode cloud model for the low- to mid-latitude regions of the planet. Possible mesoscale variation in the cloud is indicated by a comparison of the data with values from radiative transfer calculations using branching plots of radiances at two different wavelengths. When the ratio of radiances at 2.53 and 2.4 μm is approximately related to the cloud base altitude, a correlation between high base altitude and low cloud opacity is observed.

Further goals are to further investigate the differences found by Wilson et al. (2008) in the cloud structure in the polar regions, examine the effects of variations in the composition and size of cloud aerosol particles, and look for evidence of the sub-cloud haze postulated by Satoh et al. (2009). Once the model is sufficiently advanced, the eventual aim is to use it in conjunction with the *Nemesis* radiative transfer and retrieval tool (Irwin et al. 2008) to study mesoscale variations in the cloud and haze and relate such variations to dynamics, gaseous abundances and volcanism.

Contents

List of Tables

List of Figures

1 Introduction

1.1 The Planet Venus

Venus is a rocky planet of approximately the same size as the Earth, but orbiting the Sun at ∼0.72 of the Earth's orbital radius. It has an orbital period of 224 days, and a retrograde rotation with a period of 243 days. Its slow rotation results in atmospheric dynamics very different to those on the Earth.

The estimated surface temperature of a Venus in radiative equilibrium with incoming solar radiation would be ∼240 K, slightly cooler than that of the Earth. However, Venus has a massive atmosphere with a surface pressure of 90 bars, and the atmosphere is composed largely of carbon dioxide which is highly absorbing in the infrared, creating an efficient greenhouse effect. The resulting average surface temperature is closer to 740 K.

Venus is covered in a layer of cloud from ∼48–75 km. This cloud is thought to be composed of concentrated sulphuric acid droplets, although the precise composition is still uncertain. The cloud layer contributes to the extremely high bolometric albedo of Venus, which is ∼0.7. Ultraviolet features indicate the presence of an ultraviolet absorber, thought to be present at the same altitude as the cloud top. However, so far all attempts to identify the substance responsible have been unsuccessful.

The slow rotation of Venus results in an atmospheric super-rotation. Zonal wind speeds in the troposphere and mesosphere of up to 90 ms^{-1} have been recently inferred from the temperature field as measured by the Visible and Infrared Thermal Imaging Spectrometer (VIRTIS) on Venus Express by Piccialli et al. (2008). The mechanism for this super-rotation is still not understood. Above 100 km, solar heating creates a strong diurnal temperature gradient which results in a strong sub-solar – anti-solar flow. Meridional transport is dominated by a Hadley cell between the equator and ∼50° latitude. The meridional extent of the Hadley cell has been inferred from an observed decrease in cloud top altitude at ∼50° (Titov et al. 2008). This conclusion is supported by the observed increase in the concentration of carbon monoxide at 35 km altitude and ∼60° latitude, caused by a downward transport of CO-rich air with the downwelling branch of the Hadley cell (Tsang et al. 2008b), although this may be an over-simplistic interpretation as some longitudinal CO variation has also been observed (Tsang et al. 2009).

Atmospheric vortices that are most often dipolar in shape have been observed close to both poles, and these are thought to be driven by the meridional Hadley cell transport. They are characterised by infrared-bright double-eye features (Piccioni et al. 2007). The north polar dipole structure was first imaged in the far-infrared by the VORTEX instrument on Pioneer Venus (Taylor et al. 1979). The south polar vortex has been observed by VIRTIS in recent years, and found to be similar to that in the

northern hemisphere, although displaying a faster rotation speed (Piccioni et al. 2007). During the first few months of observation by VIRTIS the shape remained broadly dipolar, although a detailed double-eye structure was not always observed (Piccioni et al. 2007). The shape of these vortices has then been observed to vary between observations, and the exact mechanism for their formation is poorly understood. Similar vortices on Titan are thought to act as a mixing barrier in the stratosphere and mesosphere (Teanby et al. 2008), and it is possible that such considerations apply on Venus.

Venus has a much higher abundance of CO_2, CO and SO_2 than the Earth, but its atmosphere is much dryer. A comparison is provided below in Table 1, with values taken from Taylor & Grinspoon (2009). The reasons for these compositional differences are unclear, particularly if the initial atmospheres of Earth and Venus were identical in composition, but it is thought that the relatively high abundance of SO_2 is due to high levels of volcanic activity. Donahue et al. (1982) interpret the high deuterium-hydrogen abundance ratio as measured by the Pioneer Venus large probe mass spectrometer as evidence that Venus was once much wetter than it is today. The D/H ratio is enriched by a factor of 100 compared to that on Earth, and Donahue et al. (1982) postulate that this came about from the greater likelihood of exospheric escape of hydrogen over the heavy isotope deuterium. The high enrichment indicates that a large amount of hydrogen from the dissociation of H_2O has escaped from Venus in the past, and this is why Venus is dry. The low abundance of atmospheric CO_2 on Earth compared to that of Venus could be explained by the high uptake of CO_2 by the oceans on Earth and the subsequent formation of carbonate minerals.

	Venus	Earth
CO_2	0.96	0.003
N_2	0.035	0.770
Atomic O	trace	trace
H_2O	0.000030	∼0.01
SO_2	0.00015	0.2 ppb
CO	0.00004	0.12 ppm
Surface Pressure	92 bar	1 bar
Surface Temperature	∼740 K	∼290 K

Table 1: A comparison table for the atmospheres of Earth and Venus. Abundances are taken from Taylor & Grinspoon (2009), and are given as fractions unless otherwise specified.

Venus has the greatest number of 'volcanic' topographic features in the solar system, and areas of high surface emissivity have also been interpreted as evidence of lava flows. Radar-bright features from ground-based measure-

ments were interpreted as volcanic in origin by Saunders & Malin (1977), and the topographical maps generated using data from the Magellan probe have provided evidence that over 90% of the surface is covered by features that bear a close resemblance to volcanic features on Earth (Head et al. 1992). With data from VIRTIS, correlations between high emissivity regions and volcanic features interpreted from Magellan topography data have been observed (Helbert et al. 2008). Whereas the presence of past volcanism on Venus is widely accepted, it is unknown whether it occurred in sporadic bursts of high activity or continuously. Bullock (1997) completed evolutionary model simulations of both possibilities, and concluded that the most likely evolutionary scenario was an epoch of massive volcanic plains emplacement between 600 and 1100 million years ago, although this has been debated. Esposito et al. (1988) suggest that an observed decrease in sulphur dioxide concentration above the cloud tops during the Pioneer Venus mission could be evidence that volcanic activity has occurred more recently, possibly favouring a more constant outgassing model.

The relationship between the atmosphere of Venus and the surface mineralogy is still unknown. Hashimoto & Abe (2005) discuss the relative merits of carbonate and pyrite models for surface-atmosphere equilibrium. The carbonate model is based on the Urey equilibrium reaction (Urey 1952) as proposed by Bullock & Grinspoon (2001). This carbonate buffer reaction is

$$\mathrm{CaCO_3 + SiO_2 \rightleftharpoons CaSiO_3 + CO_2}. \tag{1}$$

However, Hashimoto & Abe (2005) believe that the amount of carbonate rock reservoir required to buffer a 90 bar atmosphere of CO_2 would be equivalent to a layer 1 km thick across the entire surface of Venus. Instead, they suggest that a pyrite equilibrium model may be more appropriate:

$$\mathrm{3FeS_3 + 16CO_2 \rightleftharpoons Fe_2O_4 + 6SO_2 + 16CO}. \tag{2}$$

As the composition of the surface rock is still unknown, however, reaching a conclusion as to the precise nature of surface-atmosphere interaction on Venus is difficult.

Venus has no significant intrinsic magnetic field, so the solar wind interacts directly with the upper atmosphere. MAG and ASPERA instruments on Venus Express will be used to investigate this interaction and the Venus plasma environment during the mission (Zhang et al. 2006).

1.2 Missions to Venus

The Venus Express satellite, launched in November 2005, is the latest in a series of successful missions to Venus that began with the flyby of the NASA Mariner 2 spacecraft in 1962. Mariner 2 data provided an indication that temperatures at the surface reached at least 700 K. Several probes

from the USSR successfully entered the atmosphere of Venus during the late 1960s, culminating in Venera 7 becoming the first probe to send a signal back from the surface of another planet. The Venera series during the 1970s provided the first in-situ data from the surface and atmosphere of Venus, including initial surface rock-type indications from radioactive species abundance, relative abundances of atmospheric constituents, initial cloud profiles and wind speed data, and confirmation that the solar flux at the surface is sufficient for a runaway greenhouse to exist (Marov 1978).

The success of these missions was followed by results from the Pioneer Venus multiprobe and orbiter mission in 1978. Collated data from this mission refined the temperature structure and atmospheric gaseous abundances obtained by the Venera probes 4–10, and also detected two regions of instability in the atmosphere where overturning can occur from 20–29 km and 52–56 km altitude (Donahue 1979). Data from orbiting infrared and ultraviolet spectrometers and the cloud polarimeter, the nephelometers, the cloud particle size spectrometer and the solar flux radiometer on the descent probes provided constraints on cloud structure and particle size. Surface topography was also observed using a radar instrument on the orbiter.

Data from these probes, combined with results from the Venera series, formed the basis for the Venus International Reference Atmosphere (Kliore et al. 1986), which is still used as an a priori for Venus atmospheric models today.

The 1985 Vega 1 and 2 lander/balloon probes close to the equator and morning terminator provided surface temperature and pressure values of 733 ± 1 K and 89 ± 1 atm respectively, as well as detecting a temperature inversion between 62 and 64 km (Petropoulos & Telonis 1988). The aim of the next mission to Venus, Magellan, was to gather radar and radiometric data from the surface in order to generate a topographical map of Venus. It also carried a gravity experiment to map the gravity field of Venus and look for anomalies that may provide an insight to the tectonic structure of the planet.

A ground-breaking discovery by Allen & Crawford (1984) opened up new possibilities for remote sensing of the clouds and lower atmosphere of Venus. Ground-based observations of Venus using the Anglo-Australian Telescope revealed the presence of 'windows' in the infrared within which the optical thickness of the Venusian atmosphere is sufficiently low that the lower atmosphere and the surface can be observed remotely.

The Venus Express orbiter is the most recent mission to Venus, and is the first to exploit these infrared spectral windows to observe the lower atmosphere from space. The varied instrumentation of this mission reflects its multiple goals. Of particular interest and relevance to this work is the Visible and InfraRed Thermal Imaging Spectrometer, VIRTIS, which is designed to provide data for surface mineralogy, cloud properties, temperature and gaseous abundances from the surface to the upper atmosphere.

2 The Venus Express Mission and Data

2.1 Venus Express

Venus Express (VEX) was launched in November 2005 and entered Venusian orbit in April 2006. The nominal mission was due to last for 2 Venus sidereal days, but has now been extended until December 2009. Seven science instruments are onboard VEX. These are the Analyser of Space Plasma and Energetic Atoms (ASPERA), a magnetometer (MAG), the Planetary Fourier Spectrometer (PFS, not useable due a a scanning fault), SPectroscopy for Investigation of Characteristics of the Atmosphere of Venus (SPICAV), the Venus Radio Science Package (VeRa), the Visible and InfraRed Thermal Imaging Spectrometer (VIRTIS), and the Venus Monitoring Camera (VMC). Data from VIRTIS has been used in this work and the instrument is described below in more detail.

2.2 The Visible and Infrared Thermal Imaging Spectrometer

VIRTIS was originally designed for the cometary mission Rosetta, to study the mineralogy and petrology of the comet P\Wirtanen (Coradini et al. 1998). It consists of three unique data channels, two of which are mapping channels, one operating in the wavelength range 0.25–1.0 μm (VIRTISM-VIS) and the other in the range 1.0–5.0 μm (VIRTISM-IR). The spectral sampling of VIRTIS-M is 0.01 μm. The third channel is devoted to spectroscopy, and is a high-resolution echelle spectrometer operating in the range 2.0–5.0 μm (VIRTIS-H). The work presented here uses data from the VIRTISM-IR channel. A schematic of the instrument taken from Coradini et al. (1999) is shown in Figure 1.

Data from the VIRTIS-M part of the instrument is transmitted as a three-dimensional cube, with two spatial dimensions and one spectral dimension. The spectrometer slit is 256 pixels across, and during each observation VIRTIS-M scans in a direction perpendicular to the orientation of the slit, recording a 256×256 pixel image. The third dimension of the cube is provided by the 432 spectral channels (Drossart et al. 2007). Geometry files are also distributed with the calibrated data, which contain geometrical data for each individual pixel. The instantaneous field of view of VIRTIS-M over the whole slit is 0.25×64 mrad, which corresponds to a distance of ∼1/3 of the diameter of the planet at apocentre. After taking into account scanning by the secondary mirror, the total field of view is 64 mrad (Drossart et al. 2007). The spectral resolution of VIRTIS-M is given by Svedhem et al. (2007) as $(\lambda/\Delta\lambda)$ ∼200, and the size of a single pixel is 0.25 mrad. This corresponds to a spatial resolution of ∼20 km even at apocentre (60,000 km from the planet).

Ten modes of observation, or science cases, were developed for Venus Express during the mission preparation. These are described in detail by

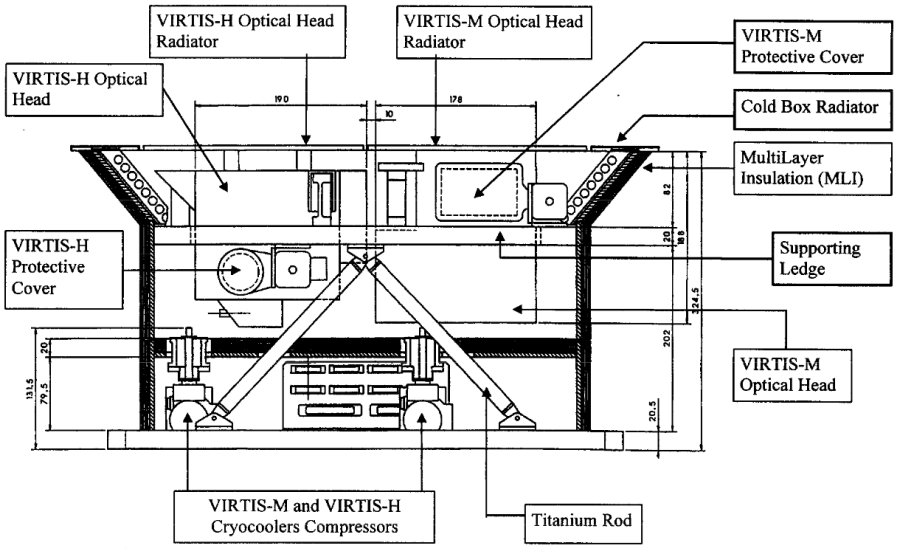

Figure 1: A schematic of the VIRTIS optics module, taken from Coradini et al. (1999).

Titov et al. (2006) and are listed below in Table 2. Out of these ten scenarios, VIRTIS is operational during cases #1, #2, #3 and #7. VIRTIS-H will be used for high resolution pericentre observations in case #1. VIRTIS-M will mainly be operational in cases #2, #3 and #7. Observations in case #7 with VIRTIS-M are in slit mode only, so no scanning is used (Drossart et al. 2007).

Case #1	Pericentre observations
Case #2	Off-pericentre observations
Case #3	Global spectro-imaging from apocentre
Case #4	VeRa bi-static sounding
Case #5	Stellar occultation by SPICAV
Case #6	Solar occultation by SPICAV/SOIR
Case #7	Limb observations
Case #8	VeRa Earth radio occultation
Case #9	VeRa solar corona experiment
Case #10	VeRa gravity experiment

Table 2: Brief descriptions of the science cases used by Venus Express.

2.3 Observations

24 observations in total were investigated in this work, obtained from eight different orbits. These observations were chosen because they are the only

observations available that have an integration time of 18 s, the longest integration time used by VIRTIS-M. These observations cover southern hemisphere latitudes from 0 – >80°, and also cover a range of viewing angles. Data investigated came from observations _00, _01 and _02 from the orbits 0319, 0320, 0321, 0334, 0344, 0359, 0373 and 0382. As three observations from each orbit were studied, there is the potential to study the evolution of particular features from observation to observation within an orbit.

3 Models of the Venus Cloud Layer

3.1 The Process of Understanding the Venus Clouds

The clouds on Venus play an extremely important role in the energy balance of the atmosphere, and so understanding them is of vital importance if we are to comprehend the evolution of the Venusian climate. The high albedo (reflectivity) of the clouds prevents much of the solar radiation from penetrating as far as the surface, and the sulphuric acid aerosol particles that form the clouds are also strong scatterers in the near-infrared and strong absorbers at wavelengths above ∼3 μm, contributing to the greenhouse effect by preventing thermal radiation from the surface from escaping into space.

After brightness temperatures derived from microwave observations provided initial evidence that the surface temperature of Venus was at least 600 K (Sagan 1960), Sagan (1962) discussed the possibility of a greenhouse model for Venus, having postulated that water vapour clouds were partially responsible for this effect (Sagan 1960). Evidence of a stronger compositional candidate for the cloud began to emerge a decade later, when Young (1973) summarised the inferred properties of the cloud particles from optical polarisation data. He concluded that the only substance consistent with the available spectroscopic and polarimetric data was concentrated sulphuric acid vapour, containing about 75% by weight H_2SO_4. Young also pointed out that the presence of sulphuric acid is to be expected on a planet with a high level of volcanic activity, as it is a naturally-occurring constituent of volcanic gas and can also be formed from other outgassed substances (water and SO_2). He concluded that other suggestions such as the acids HCl, HF and HNO_3 could be ruled out, at least as candidates for the upper cloud layer.

This conclusion is supported by the work of Pollack et al. (1974), who interpreted reflectance spectra in the 1.2–4.1 μm wavelength region as also indicative of a sulphuric acid cloud layer. Pollack et al. compared Venus reflectance spectra with synthetic spectra for several possible candidates and determined that the only substance that matched a cloud absorption feature between 3 and 4 μm was a solution of H_2SO_4, with a concentration of 75 % by weight or higher. It was, however, not possible to distinguish between solutions of 75 and 95 wt % using these data. The possibility of impurities

being present in the aerosol particles was invoked to explain a poor match between H_2SO_4 synthetic spectra and data in the ultraviolet region of the Venus spectrum.

The Pioneer Venus mission, described in detail by Colin (1980), had a range of instruments on an orbiter and several descent probes devoted to studying the Venusian cloud. These were the nephelometers on the large and small descent probes (LN/SN), the Large Probe Cloud Particle Size Spectrometer (LCPS) and the Orbiter Cloud PhotoPolarimeter (OCPP). The five descent probes entered the atmosphere at different locations. These consisted of three small probes, one entering the dayside (Day) atmosphere, one the nightside (Night) and the third entering the atmosphere at around 60° latitude in the northern hemisphere (North). A large probe (Sounder) and the bus on which the probes were mounted also entered the atmosphere. The cloud vertical profiles obtained by these probes were generally in good agreement with similar profiles derived from backscattering nephelometer data from the Venera 9, 10, 11, 13 and 14 probes, although some variations in the cloud base and cloud top regions were noticeable (Kliore et al. 1986).

The LCPS instrument provided a vertical profile of the cloud, distinguishing between three different aerosol particle size modes. These modes range from mode 1, the smallest, to mode 3, the largest. Kliore et al. (1986) includes a plot, reproduced below (Figure 2), of the vertical distribution of these three particle modes at the LCPS descent site.

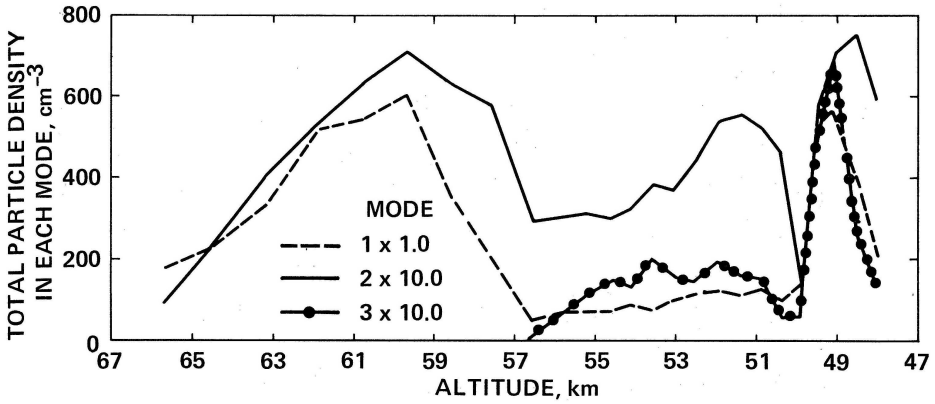

Figure 2: Particle number densities in the three size modes obtained from LCPS data, as presented in Kliore et al. (1986).

The question of possible impurities in the cloud particles was revisited after results from the Pioneer Venus mission became available. Cimino (1982) examined data from the radio occultation experiment, and modelled the aerosol particles as a solid dielectric sphere with a coating of liquid sulphuric acid. This increases the absorptivity of the particles compared to a

pure sulphuric acid sphere. The mass contents she derived from the radio occultation data, assuming liquid concentrated H_2SO_4 aerosols, are more than an order of magnitude greater than mass contents determined by the LCPS, which suggested that particles with a higher absorptivity were required. The spectral dependence of the absorption coefficient determined for the occultation data was also found to be different from that of liquid H_2SO_4. She concluded that the best-fit model consisted of a solid core making up 97 % of the particle by radius, with a thin coating of liquid H_2SO_4.

It is now known that the cloud opacity is highly variable, so a cloud mass content observed at one time and in one place could very conceivably differ by an order of magnitude from a content observed elsewhere. However, we cannot yet rule out the possibility of impurities in the cloud particles as the nature of the ultraviolet absorber in the cloud top regions remains unknown. The composition of the largest cloud particles in the lower cloud is also a subject of debate. Esposito et al. (1983) suggested chlorides such as HCl or $FeCl_3$ instead of H_2SO_4, or $NOHSO_4$.

Current observations by VIRTIS allow the study of the Venusian cloud using the infrared window regions discovered by Allen & Crawford (1984) between 1.0 and 2.6 μm. Radiance at these wavelengths is heavily attenuated by the cloud and as such measurements at these radiances provide a good indication of cloud opacity (Figure 3). It has become apparent that alterations in mean particle size and base altitude can also have a significant effect on the measured spectra from Venus (Carlson et al. 1993, Wilson et al. 2008, Satoh et al. 2009). The cloud can also be sounded using the VMC, which monitors the cloud top in the ultraviolet and VeRa, which provides radio occultation profiles of the neutral atmosphere. A schematic diagram of the Venusian cloud is given in Figure4.

3.2 Clouds in Radiative Transfer Models

A detailed cloud model, based on data from the OCPP, LCPS and Solar Flux Radiometer was used by Crisp (1986) in his radiative transfer model of the Venus atmosphere. His cloud model consists of four H_2SO_4 aerosol particle modes, with radii for each mode listed in Table 3. An upper haze is present between 80 and 90 km, the upper cloud above $\sim$ 57 km has a bimodal distribution of mode 1 and mode 2 particles, and the lower cloud from $\sim$ 48–57 km has a trimodal particle distribution of modes 1, 2 and 3 (mode 2' is treated as a tail of the mode 2 size distribution but is restricted to the middle and lower cloud layer). The ultraviolet absorber is incorporated into the mode 1 particles in the upper clouds.

Crisp's cloud model is characterised by a lower cloud for which aerosol particle abundance does not decrease noticeably with height, and an upper cloud with a scale height of the same order as the atmospheric scale height. These vertical distributions and size distributions are based on the inter-

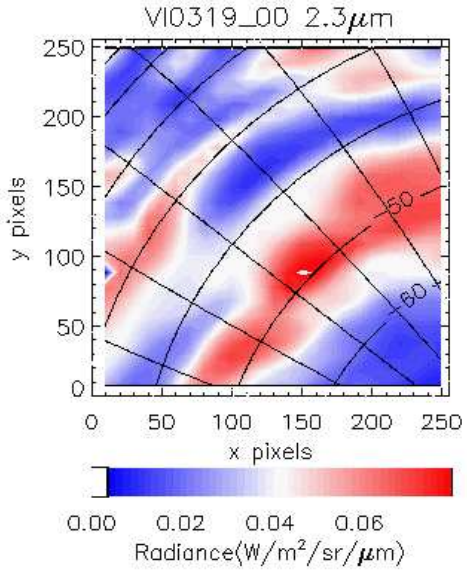

Figure 3: An image of Venus at 2.3 μm, plotted using VIRTISM-IR data from the observation 0319_00. The data have been coadded spatially in bins of 20 $\times$ 20 pixels, at 10 pixel intervals. Blue corresponds to thick cloud and low radiance, whilst red indicates thin cloud and high radiance.

Mode	Effective Radius at Equator (μm)	Eff. Rad. at Poles (μm)
Mode 1	0.49	0.29
Mode 2	1.18	1.01
Mode 2'	1.40	1.40
Mode 3	3.65	3.65

Table 3: Aerosol particle size distribution as used in the radiative transfer model of Crisp (1986).

pretation of results from the Pioneer Venus OCPP and LCPS experiments, data from both being used to constrain optical depths for the upper cloud and LCPS data being used for the lower cloud.

This model was further developed by Pollack et al. (1993), incorporating data from the Galileo/NIMS flyby. In their model spectra for the nightside of Venus, mode 2 particles are restricted to the upper cloud only, whilst mode 2' and mode 3 are restricted to the lower cloud. Opacity profile modifications were made in order to bring the model into better agreement with the NIMS data.

A similar parameterisation was produced by Grinspoon et al. (1993). They generated a best-fit vertical cloud model by comparing synthetic limb-

darkening curves with those obtained from the Galileo/NIMS data. They found that the data were fit best by a model in which the upper cloud optical depth remains constant, and the majority of the cloud opacity variation occurs in the region from 48–50 km. The results from Grinspoon et al. (1993) and Pollack et al. (1993) are similar, and favour a three- or four-mode cloud model with larger mode 3 particles towards the bottom of the cloud. The nominal cloud base is given in Pollack et al. (1993) as 48 km. Further evidence for a cloud base of ∼48 km is provided by the Pioneer Venus descent probe results, as summarised in Kliore et al. (1986), and in Mariner 10 data reanalysed by Kolodner & Steffes (1998).

All three models described above used refractive index data for sulphuric acid obtained from laboratory measurements by Palmer & Williams (1975). These data were used, together with the assumed size distributions, to calculate the extinction coefficient and single scattering albedo for each mode at each wavelength. The derived scattering properties were then included in the radiative transfer model. Grinspoon et al. (1993) used values 84.5 and 95.6 wt % H_2SO_4 as opposed to the 75 wt % used by Crisp (1986) and Pollack et al. (1993). Palmer & Williams (1975) provide optical data for these three concentrations. Distinguishing between different concentrations of acid using observational data is not straightforward as the problem is underconstrained.

There are other sources of uncertainty for such models. No data was available between the cloud top and the 75 mbar level at the time of Crisp's model, mode 1 particles were too small to be detected by the LCPS instrument, and the extrapolation of a model based on descent probe data to a planet-wide scale is based on the potentially flawed assumption that the conditions at the probe entry site and time were typical. However, the Galileo/NIMS data provided an opportunity to refine this model using remote-sounding data obtained over a wider area of the planet, and went some way towards removing these uncertainties. The Crisp model as refined by Pollack et al. (1993) and the model of Grinspoon et al. (1993) together gave the most accurate representation of the Venusian cloud that was possible with the data available at the time, showing significant agreement despite different approaches, and therefore these models have been used as a starting point for those developed in this work.

New possibilities were opened up with the data obtained by Venus Express. Satoh et al. (2009) postulate that there may be small haze particles as low in the atmosphere as 30 km, based on a best-fit forward model of the shape of the 1.74 μm peak, but if so these particles cannot be made of concentrated sulphuric acid as sulphuric acid vapour is expected to decompose into SO_3 and H_2O at temperatures found below 45 km altitude on Venus (Prinn 1978). Also, the possibility of alterations in the average particle size across the planet is explored by Wilson et al. (2008), after initial findings by Carlson et al. (1993). They find that the ratio of the peak radiances at

1.74 and 2.3 μm is indicative of a 'size parameter' for a cloud model with a single-mode size distribution. When the results of this model are compared with VIRTISM-IR data, they find that the average particle size is constant over the majority of the planet but increases towards the poles, indicating that cloud formation processes are different at latitudes greater than 60°, possibly as a result of a different convective regime. Erard et al. (2009) suggest that their independent component analysis of VIRTIS spectra indicates variation in particle size within the polar region, with regions of different average particle size forming concentric rings around the polar vortex.

3.3 The Current Oxford Cloud Model

The current cloud model in use at Oxford is based on the model of Pollack et al. (1993), with a few modifications (detailed in Section 6). It has four particle modes and, as with Pollack et al. (1993), restricts modes 2' and 3 to the lower cloud and mode 2 to the upper cloud. The size distribution is given in Table 4, and all modes are treated as having a log-normal distribution, as in Pollack et al. (1993). The refractive index data used to generate scattering cross-sections and extinction coefficients is that of Palmer & Williams (1975). A composition of 75 wt % H_2SO_4 is assumed for all size modes. This choice of concentration is the same as that of Pollack et al. (1993), Kamp & Taylor (1990), Meadows & Crisp (1996) and Marcq et al. (2005), facilitating comparison of the models. However, the results of Grinspoon et al. (1993) favour a higher concentration, which cannot be ruled out and requires further investigation.

Mode	Effective Radius(μm)	Width of Distribution (μm)
Mode 1	0.30	0.44
Mode 2	1.00	0.25
Mode 2'	1.40	0.21
Mode 3	3.65	0.25

Table 4: Aerosol particle size distribution as used in the Oxford radiative transfer model for Venus.

4 Cloud Microphysics

4.1 Cloud formation on the Earth

Cloud formation on the Earth can be used as a useful illustration for the sort of physical processes that may cause the formation of cloud on Venus. Cloud formation on the Earth relies on convective processes. Parcels of moist air rise due to convection in the atmosphere, and when the temperature of such a parcel falls below the dew point temperature it reaches saturation

with respect to water (Rogers & Yau 1989). Once saturation is achieved, water vapour can condense out and form cloud droplets, provided there are sufficient cloud condensation nuclei.

Adiabatic expansion/contraction of dry air can be described using the first law of thermodynamics. In differential form, this can be stated as

$$\mathrm{d}q = c_p \mathrm{d}T - \alpha \mathrm{d}p, \tag{3}$$

where $\mathrm{d}q$ is the change in heat per unit mass, c_p is the specific heat capacity for constant pressure, T is temperature, $\mathrm{d}p$ is change in pressure and α is the volume per unit mass. For an adiabatic process, we can set $\mathrm{d}q$ to zero. If, however, the air is not dry but moist, we have to take into account the effect of water on these processes. When water is in the vapour phase, we can treat it as an ideal gas (Rogers & Yau 1989), so we can use the equation of state for an ideal gas to define the vapour pressure, e:

$$e = \rho_v R_v T, \tag{4}$$

where ρ_v is the density of the water vapour and R_v is the individual gas constant for water vapour.

The evaporation of water requires heat. The latent heat of vaporisation is the heat energy required to convert a unit mass of water into water vapour, if there is no change in the pressure or temperature. The latent heat L is given by

$$L = \int_{q_1}^{q_2} \mathrm{d}q = \Delta u + e_s \Delta \alpha, \tag{5}$$

where e_s is the vapour pressure at which the air is saturated with respect to water vapour and Δu is the change in internal energy between the two states. Given that we have assumed T is constant, we can also write this as

$$L = T \int_{q_1}^{q_2} \frac{\mathrm{d}q}{T} = T \Delta s, \tag{6}$$

where s is the entropy per unit mass. Equating (5) and (6) allows us to find a conserved thermodynamic quantity that we will call the Gibbs free energy G:

$$G = u + e_s \alpha - Ts. \tag{7}$$

Conservation of the differential $\mathrm{d}G$ leads to the Clausius-Clapeyron equation, given below:

$$\frac{\mathrm{d}e_s}{\mathrm{d}T} = \frac{\Delta s}{\Delta \alpha} = \frac{L}{T \Delta \alpha}. \tag{8}$$

The saturation vapour pressure defines the point at which condensation of water vapour is energetically favourable, and the Clausius-Clapeyron equation gives the temperature dependence of this quantity. Thus, the predominant mechanism on the Earth for creating supersaturations is cooling.

However, this rather simplistic model does not entirely describe the full requirement for cloud formation. The Clausius-Clapeyron equation does not take into account the free energy barrier for condensation of water into small droplets (Rogers & Yau 1989), so in fact condensation into droplet form might not be expected to occur until large supersaturations of water vapour are reached. In reality, we do observe the formation of cloud particles for small supersaturations because the air is full of micron and sub-micron particles that act as a source of cloud condensation nuclei (CCN), facilitating droplet formation without the need for large supersaturations.

The saturation vapour pressure for a spherical droplet is dependent on the radius of curvature, and is given below by the Kelvin equation:

$$e_s(r) = e_s(\infty)\exp\left(\frac{2\sigma}{R_v\rho_l T r}\right), \tag{9}$$

where r is the radius of curvature of the droplet, σ is the surface tension and ρ_l is the density of the liquid. A droplet must therefore achieve a critical size if it is to be stable, as the vapour pressure must equal this saturation vapour pressure for the rates of evaporation and condensation to be balanced (Rogers & Yau 1989). Particles greater than this size are said to be 'activated' and it is favourable for them to grow by condensation. Formation of droplets of the critical size can occur by a variety of processes, listed by Houze, Jr. (1993). The growth of a drop of pure water by condensation alone is homogeneous nucleation, whereas the growth of a droplet around an aerosol particle is heterogeneous nucleation. Heterogeneous nucleation is by far the more important of these two processes on Earth. Cloud droplets can also grow when smaller droplets collide and coalesce, which is best modelled as a discrete process called stochastic collection. This model results in a more realistic size distribution than an assumption of continuous growth as it takes into account the possibility that two drops of the same initial size may not attain the same size after a time Δt, as they may experience different numbers of collisions.

4.2 Cloud Microphysics on Venus

The mechanisms for cloud formation on Venus are poorly understood compared with those on Earth, but the theory above can still be applied. A very simple cloud formation process for Venus is outlined in Figure 4.

A multi-modal distribution as observed in the Venus cloud favours a stochastic collection model for the initial growth and activation of cloud droplets. Knollenberg & Hunten (1980) suggest that the smallest mode 1 particles have not yet reached the critical radius and are not yet activated, so remain small as they can only grow by coalescence, whereas mode 2 particles have achieved this critical radius and so can grow to larger sizes more easily, explaining the marked difference in average size between these

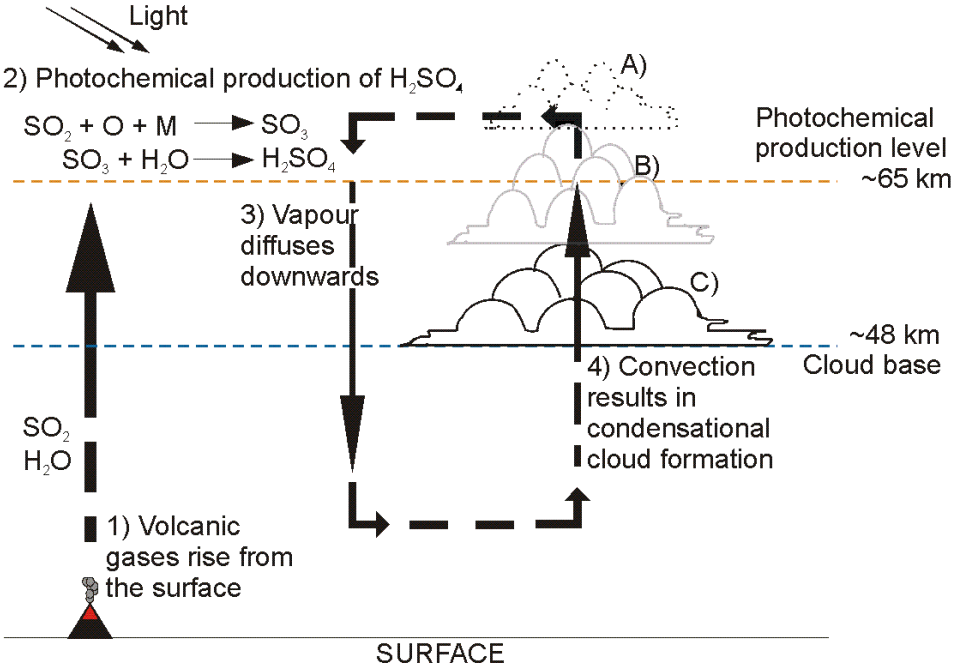

Figure 4: A simple schematic of how sulphuric acid clouds may form on Venus. A) marks the upper haze, B) is the upper cloud composed of mode 1, mode 2 and UV absorber particles, and C) is the lower cloud made mostly of mode 2' and mode 3 particles, as described by Crisp (1986) and Pollack et al. (1993).

two modes. Cloud condensation nuclei are believed to be an important part of this process - indeed, Knollenberg & Hunten (1980) suggest that the smallest mode one particles detected by the Pioneer Venus LCPS in the lower cloud may be just bare CCN, with little sulphuric acid content. Imamura & Hashimoto (2002) assume the CCN to be made of elemental sulphur, with a single radius of 0.17 μm, based on the LCPS measurements discussed by Knollenberg & Hunten (1980).

The formation mechanism for mode 3 particles is less certain. Knollenberg & Hunten (1980) suggest that these particles may be crystalline. Other models treat all modes as composed of concentrated sulphuric acid (see Section 3). The model of Imamura & Hashimoto (2002) results in mode 3-sized particles being produced by condensation of sulphuric acid as a result of vigorous diffusion in the region of the lower clouds.

Bullock (1997) in his thesis on the stability of the Venusian climate utilised a simple chemical and microphysical model for cloud feedback processes. This model took into account the photochemical formation of H_2SO_4 aerosols and the subsequent diffusion/convection/condensation processes as

shown in Figure 4. A relationship between particle size and number density was obtained by setting equal the Stokes drift timescale of the particles and the Brownian coagulation timescale of aerosols. The aerosol vapour was assumed to be destroyed at a temperature of 432 K, which occurs around 40 km altitude. The resulting particles were then binned according to size and composition, and this distribution was used in the radiative transfer calculations.

McGouldrick & Toon (2007) and McGouldrick & Toon (2008) also implement a microphysical cloud model to investigate the mesoscale spatial evolution of the Venus condensational clouds. They use the Community Aerosol and Radiation Model for Atmospheres (CARMA) to investigate the evolution of 'holes' in the cloud and the effect of convection cells and gravity waves. The use the values of Knollenberg & Hunten (1980) at 40 km as the CCN input distribution for their microphysical model.

The results of these different microphysical models suggest that simple microphysical parameterisations can be useful in modelling the behaviour over time of the Venusian cloud. The work of Knollenberg & Hunten (1980) provides a good physical basis for a multi-modal cloud as observed on Venus. In summary, it seems likely that the size distribution on the Venusian cloud is achieved through stochastic collection followed by preferential condensational growth of larger particles, although this does not rule out the possibility that the mode 3 particles may have an entirely different origin.

5 Retrieval Theory and *Nemesis*

Remote sensing is an extremely useful method of studying planetary phenomena over large areas and obtaining coverage of these phenomena on planet-wide scales. In this work, I will be using VIRTIS measurements of infrared radiation from the surface and lower atmosphere of Venus to derive properties of the cloud. I will use the radiative transfer and retrieval tool, *Nemesis* (Irwin et al. 2008), to create model Venus spectra for the wavelength range of VIRTIS-M in which the window regions discovered by Allen & Crawford (1984) reside ($\sim$1.0–2.6 μm).

Nemesis (Irwin et al. 2008) was created as a retrieval code that could be used to model any planet and data from any instrument. The acronym stands for Non-linear optimal Estimator for MultivariatE spectral analySIS. It uses a non-linear optimal estimator formalism to find the best-fit forward model to a spectrum for up to four different variables simultaneously, allowing the solution of an under-constrained problem.

Performing a retrieval involves the generation of a radiative transfer model using a set of a priori values for various parameters. The model spectrum generated may be sensitive to some or all of these parameters in certain wavelength regions. The *Nemesis* tool uses code derived from

RADTRANS to generate radiative transfer models. The input for *Nemesis* for Venus currently uses pressure and temperature values from the models of Seiff et al. (1985) to form vertical profiles of 111 altitude levels, ranging from the surface to 150 km. Seiff et al. (1985) used collected data from the Pioneer Venus probes and orbiters and Veneras 10, 12 and 13 to obtain optimal model profiles. Gaseous abundance vertical profiles are taken from Kliore et al. (1986), and vertical profiles for four cloud modes are used. The cloud model is described in more detail in Section 6. *Nemesis* calculates the spectral radiance leaving the atmosphere at the desired spectral resolution, allowing the calculation of forward models to simulate results from a range of instruments.

Radiative transfer models are calculated by solving the equation of radiative transfer (10) for a given set of initial values for each variable parameter:

$$L_\nu = B_\nu(T_0)\tau_\nu(0) + \int_{\tau_\nu(0)}^{1} B_\nu(T)\,\mathrm{d}\tau_\nu(z). \tag{10}$$

In Equation (10), L_ν is the resulting spectral radiance after radiation has passed through an atmosphere from the surface to altitude z. $B_\nu(T_0)$ is the Planck function at surface temperature T_0 and wavenumber ν, $B_\nu(T)$ is the Planck function at temperature T for an altitude z, $\tau_\nu(z)$ is the optical depth at altitude z and $\tau_\nu(0)$ is the total optical depth of the atmosphere. The first term in the equation represents the attenuation of radiation in a beam from the surface to altitude z by the intervening atmosphere, and the second term represents radiation emitted by the gas within the beam or scattered into the beam.

Clearly, the solution to this equation requires knowledge of the strengths and positions of absorption lines for gaseous constituents in the atmosphere. If the gaseous absorption for a wavenumber region $\nu \rightarrow \nu + \Delta\nu$ is calculated by taking into account the exact contribution for each individual absorption line this is very time-consuming, and as several iterations are required before the best-fit model is calculated it is very inefficient. Two possible approximate methods can reduce computation time significantly, and these are the band model approximation and the correlated-k approximation. The band model approximation cannot be used in a scattering atmosphere, and as the clouds on Venus are strong scatterers in the VIRTIS wavelength range the correlated-k approximation, originally used by Lacis & Oinas (1991), is the only valid option.

The correlated-k approximation assumes that the precise location of an absorption line of absorption coefficient k within a small frequency interval $\nu \rightarrow \nu + \Delta\nu$ is of no importance to the calculation of the transmission in that interval. It is in fact sufficient to know what fraction of the frequency domain $f(k)\mathrm{d}k$ is occupied by absorption coefficients between k and $k + \mathrm{d}k$ (Irwin et al. 1997). Then, the mean transmission within this interval can be

written as:

$$\bar{T}(m) = \int_0^\infty f(k) e^{(-km)} \mathrm{d}k \tag{11}$$

where m is the number of molecules per square metre of atmosphere. Equation (11) has the form of a standard Laplace transform of the frequency distribution of k, and it is independent of the ordering of the absorption coefficients. Therefore we can define the cumulative frequency distribution

$$g(k) = \int_0^k f(k) \mathrm{d}k \tag{12}$$

and if Equation (12) is inverted such that $k(g) = g^{-1}(k)$ then we can rewrite $\bar{T}(m)$ as

$$\bar{T}(m) = \int_0^1 e^{(-k(g)m)} \mathrm{d}g. \tag{13}$$

If we divide the space between $g = 0, 1$ into N intervals such that g is well-sampled, we can then express $\bar{T}(m)$ as a sum rather than an integral:

$$\bar{T}(m) = \sum_i^N e^{(-\bar{k}_i m)} \Delta g_i. \tag{14}$$

This is valid for a homogeneous path through an atmosphere. In reality, such paths are inhomogeneous, and this inhomogeneity can be approximated by adding homogeneous layers together. The transmission within each layer is generally well-correlated with the transmissions in adjacent layers, so this approximation is valid. The name 'correlated-k' arises from this fact (Tsang 2007). The distribution $k(g)$ can be calculated and used as an input to the radiative transfer model, resulting in a fast forward model calculation.

Line strength data for different modes of common atmospheric gases are obtained from laboratory measurements, although for a planet such as Venus some degree of extrapolation in temperature and pressure may be required as the conditions are very different from those on Earth. The correlated-k tables for Venus are created using data from two main databases (Tsang et al. 2008a). These are HITEMP, referred to by Pollack et al. (1993) (no specific publications exist), and HITRAN2K (Rothman et al. 2003). CO_2 values from HITEMP are used, as this database contains weak rotational lines and bands that become important at high temperatures and are absent in HITRAN2K (Tsang 2007). Both Pollack et al. (1993) and Tsang (2007) find that simulations using HITEMP data are much improved over simulations using only HITRAN CO_2 lines. All other gaseous parameters are taken from HITRAN2K.

Once the initial forward model is calculated in a retrieval run, an iterative approach is used to alter a user-specified selection of the input parameters

such that an optimal fit to the data is achieved. The best-fit values for each parameter are then returned.

Non-linear optimal estimation is complex. For a linear problem, we can represent the measured properties of an atmosphere $\mathbf{y}$, in this case the radiation emitted at different wavelengths, as some function of a set of variables such as pressure, temperature, gaseous abundances etc. which we will call $\mathbf{x}$, plus a term ϵ arising from the measurement errors:

$$\mathbf{y} = \mathrm{F}(\mathbf{x}) + \epsilon. \tag{15}$$

If we ignore non-linear terms in $\mathrm{F}(\mathbf{x})$, we can write Equation (15) as

$$\mathbf{y} - \mathbf{y}_a = \mathbf{K}(\mathbf{x} - \mathbf{x}_a) + \epsilon, \tag{16}$$

where subscript $_a$ denotes an a priori vector. This cannot be solved for $\mathbf{x}$ by simple inversion as the problem will suffer from ill-conditioning — errors in the measured values will propagate and lead to unphysical solutions. Instead, an optimal estimation method is required. For non-linear optimal estimation where the problem is close to being linear, the Gauss-Newton method can be used (Rodgers 2000). This method is valid if the second derivative of the forward model $\nabla_{\mathbf{x}}\mathbf{K}^T$ is small, as in the moderately linear case, and it provides an iterative solution for $\mathbf{x}$ as shown below. The equation given in Irwin et al. (2008) is

$$\mathbf{x}_{n+1} = \mathbf{x}_0 + \mathbf{S}_x\mathbf{K}_n^T(\mathbf{K}_n\mathbf{S}_x\mathbf{K}_n^T + \mathbf{S}_\epsilon)^{-1}(\mathbf{y}_m - \mathbf{y}_n - \mathbf{K}_n(\mathbf{x}_0 - \mathbf{x}_n)), \tag{17}$$

where $\mathbf{y}_m$ and $\mathbf{y}_n$ are the measured spectrum and the spectrum calculated from the trial atmosphere respectively, $\mathbf{x}_n$ and $\mathbf{x}_0$ are the model and a priori state vectors, $\mathbf{K}_n$ is the matrix of functional derivatives, $\mathbf{S}_\epsilon$ is the measurement covariance matrix and $\mathbf{S}_x$ is the a priori covariance matrix. The covariance matrices represent the errors in the measurements and forward model ($\mathbf{S}_\epsilon$) and the errors in the a priori state vector ($\mathbf{S}_x$).

The difference between the calculated and measured spectra is minimised when the cost function given by Irwin et al. (2008) is minimised. The cost function ϕ is given by

$$\phi = (\mathbf{y}_m - \mathbf{y}_n)^T\mathbf{S}_\epsilon^{-1}(\mathbf{y}_m - \mathbf{y}_n) + (\mathbf{x}_n - \mathbf{x}_0)^T\mathbf{S}_x^{-1}(\mathbf{x}_n - \mathbf{x}_0). \tag{18}$$

The matrix of functional derivatives $\mathbf{K}_n$ represents the change in radiance at each wavelength for a change in any given input parameter — for example, a change of 1 ppmv in a gaseous abundance or a 1 K change in temperature. If a continuous vertical profile of gas or temperature is fitted, the covariance matrix is an indicator of the sensitivity to the gaseous abundance/temperature at each vertical level and each spectral interval in the model.

Nemesis has the capability to retrieve up to four different variables such as H_2O abundance, temperature and cloud distribution using various different parameterisations. For example, *Nemesis* can retrieve a continuous H_2O vertical profile, or it can simply retrieve a scaling factor for an existing a priori vertical distribution. In addition, *Nemesis* can be used to perform multi-stage retrievals, so one parameter (for example the cloud opacity) can be retrieved using one part of a spectrum, then this value can be fixed and another part of the spectrum used to simultaneously retrieve three or four gaseous abundances. The errors from the first part of the calculation are taken into account in the second stage.

The Venusian cloud is treated by *Nemesis* as a collection of highly-scattering spherical particles with a given size distribution. Mie scattering theory is used to determine the scattering properties of the Venus cloud particles, as the particle size is comparable to the wavelength in the infrared. The Henyey & Greenstein (1941) approximation to the full Mie-scattering phase function has been used in the Nemesis calculations to save on computation time. The Henyey-Greenstein phase function approximation used here is given by

$$P(\theta) = \frac{1}{4\pi}\left[f\frac{1-g_1^2}{(1+g_1^2-2g_1 cos\theta)^{3/2}} + (1-f)\frac{1-g_2^2}{(1+g_2^2-2g_2 cos\theta)^{3/2}}\right], \quad (19)$$

where θ is the scattering angle, f has a value between 0 and 1 and g_1 and g_2 are asymmetry parameters, measures of the anisotropy of the scattering. The two terms in the equation represent the forward- and backward-scattering peaks respectively.

6 Improving the Oxford A Priori Cloud Model

The cloud model forms a crucial part of any radiative transfer model for Venus, and a well-constrained cloud model is therefore necessary for retrievals of gaseous abundances below and within the cloud. The 2.3 μm window region is particularly useful for constraining gaseous abundances, as the 2.3 μm peak itself is sensitive only to the cloud opacity, whilst the region between 2.3 and 2.5 μm is sensitive to CO, H_2O and OCS. This means that the cloud opacity can be constrained independently of the gaseous absorption, which can then be investigated. However, this is of course only useful if the cloud model is sufficiently realistic.

My initial work has taken the form of improving the current Oxford cloud model. Problems with this model in the 2.3 μm window region had become apparent when models with a high input cloud opacity were created. The shape of the model in this region became distorted with respect to the observed spectral shape when the number of particles in the lower cloud was increased (Figure 5).

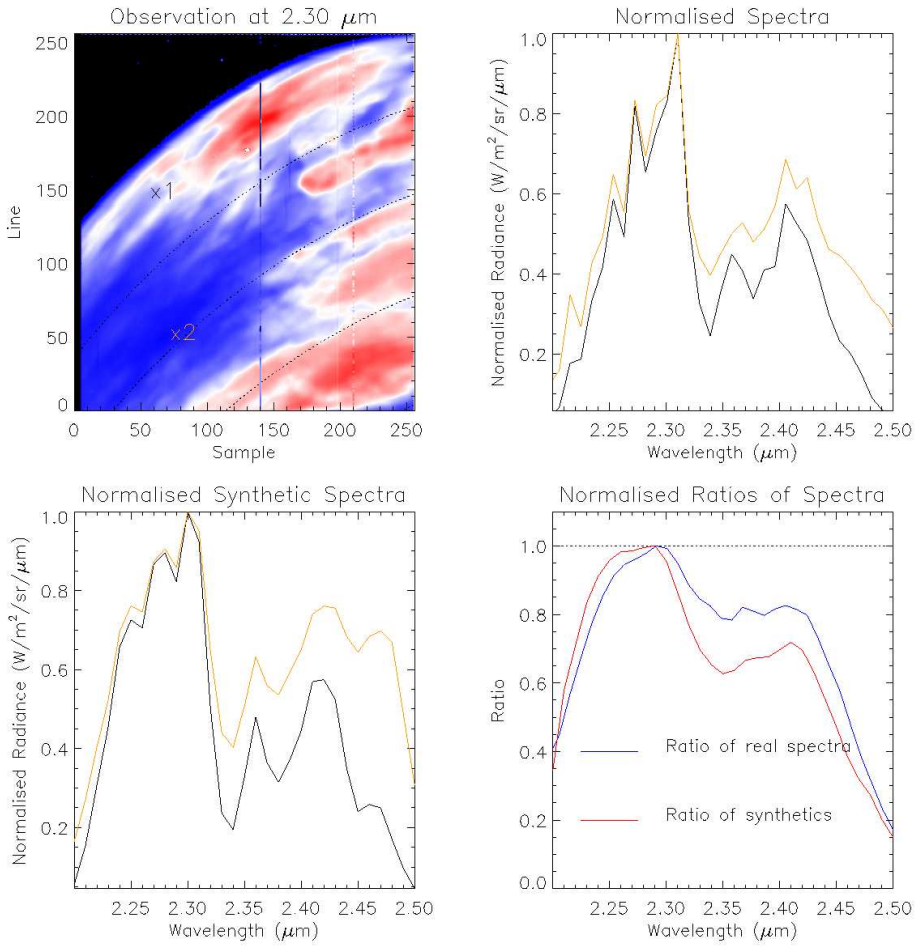

Figure 5: A comparison of data from the VIRTISM-IR observation 0321_02 with radiative transfer models of a similar radiance. A discrepancy in the behaviour can be seen at 2.47 microns, where the model radiance is too high for the example with the lower peak radiance and higher cloud amount (orange lines).

Several possibilities for the cause of the observed discrepancy were investigated. It appears from the plot that there is some significant emission in the model from the cloud at 2.47 μm when the number density of cloud particles is high, which could be caused by several factors. Uncertainties are present in the current a priori values as based on the Pollack et al. (1993) cloud model, which was discussed in Section 3. Likely errors in parameters derived from previous observational data that may produce this effect are as follows:

1. The optical data from Palmer & Williams (1975) shows that the

aerosol particles are not completely scattering in the wavelength range of interest. Large fractional errors in the imaginary refractive index in this wavelength range may result in an incorrect value for the calculated single-scattering albedo.

2. An increase in the size of the largest mode 3 particles would alter the scattering properties of these particles and this may affect the shape of the spectrum. The exact size of these particles is not well known.

3. Using a different concentration of H_2SO_4 for the largest particles may alter the model spectrum, and the exact concentration is not well-determined. Previous models have used a range of concentrations from 75 wt % to 96 wt % (see Section 3).

4. The vertical distribution of the cloud has only been directly measured by a series of descent probes, which provide information only for a specific place and time. Whilst different descent probe profiles show significant agreement, there are also some discrepancies, as noted by Kliore et al. (1986). Altering the scale height and/or base altitude of the lower cloud will change the number of cloud particles present in the line-forming region, which in turn would have an effect on the emission observed at 2.47 μm.

These possible sources of error were investigated in turn by altering the relevant input parameters to the model and seeking a solution with a generally better fit to the data by eye. The initial altitude ranges and scale heights for the four cloud modes are given below in Table 5.

Mode	Base Pressure (atm)	Top Pressure (atm)	Frac. Scale Height
Mode 1	1.6	0.0017	1.0
Mode 2	0.116	0.0017	1.0
Mode 2'	1.4	0.389	1.0
Mode 3	1.4	0.389	1.0

Table 5: Vertical distribution of the cloud modes in the initial model.

6.1 Refractive Index Data

The process of obtaining laboratory refractive index data for sulphuric acid aerosol is complex, and therefore the absolute reliability of the Palmer & Williams (1975) data for use in our cloud model is perhaps questionable. The uncertainty given for the imaginary part of the refractive index k in particular is high when k is small, so in the wavelength range of interest this uncertainty will be significant.

Another set of refractive index data that covers the major window regions in the infrared is presented by Myhre et al. (2003). These data were used

to generate new extinction cross-section and single-scattering albedo values to use as inputs for a forward model calculation. Myhre et al. (2003) used a Fourier Transform Spectrometer, unlike the single-beam spectrometer used by Palmer & Williams (1975) (Rusk et al. 1971). The spectral range used was also different to that of Palmer and Williams, starting from 1.33 μm as opposed to 0.63 μm.

The extinction cross-section and single-scattering albedo calculated using the two data sets for the lower cloud modes are shown below in Figure 6. It can be seen that the single-scattering albedo is considerably lower for the Myhre et al. data set towards shorter wavelengths, and this results in an unrealistically small radiance peak in the 1.74 μm window relative to the 2.3 μm peak when these data are used to calculate a forward model. Using this new dataset does not improve the quality of our model, and it is possible that the short wavelength cut-off in these data at 1.33 μm makes the short wavelength results unreliable.

No other datasets in the correct wavelength range at the correct temperatures and pressures are available.

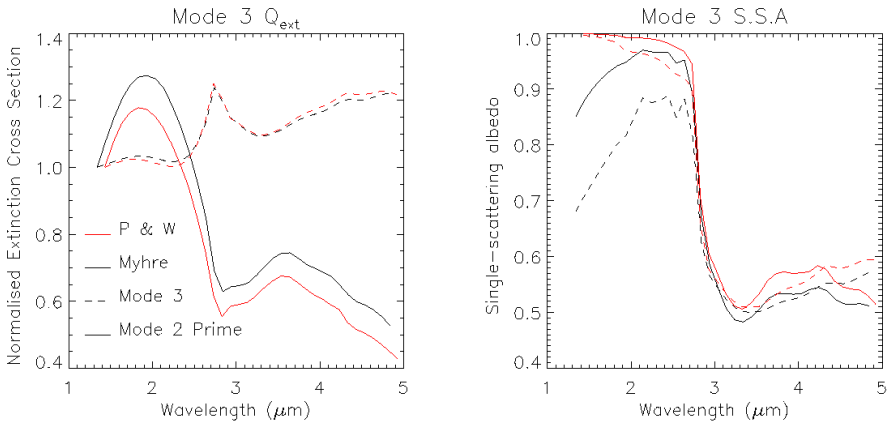

Figure 6: A comparison of extinction cross-section and single-scattering albedo generated from two different refractive index datasets by Palmer and Williams (1975) and Myhre et al. (2003).

6.2 Mode 3 Size Distribution

The precise size distribution for the large mode 3 particles is uncertain, so it is possible that the discrepancies between our model and the data arise from this. We know these particles are large compared with the other three modes, so increasing their modal size from the nominal value (see Table 4) was another possibility for improving our model.

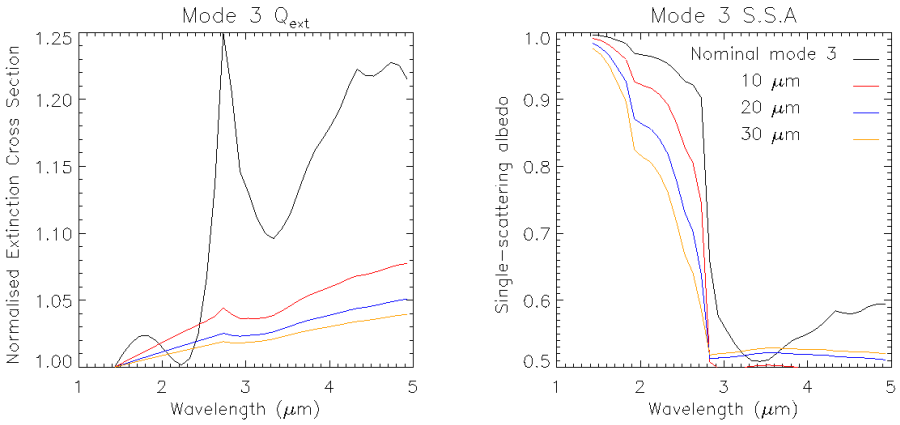

Figure 7: A comparison of extinction cross-section and single-scattering albedo generated for four different modal sizes for mode 3 particles. Increasing the particle size decreases the single-scattering albedo and extinction cross-section.

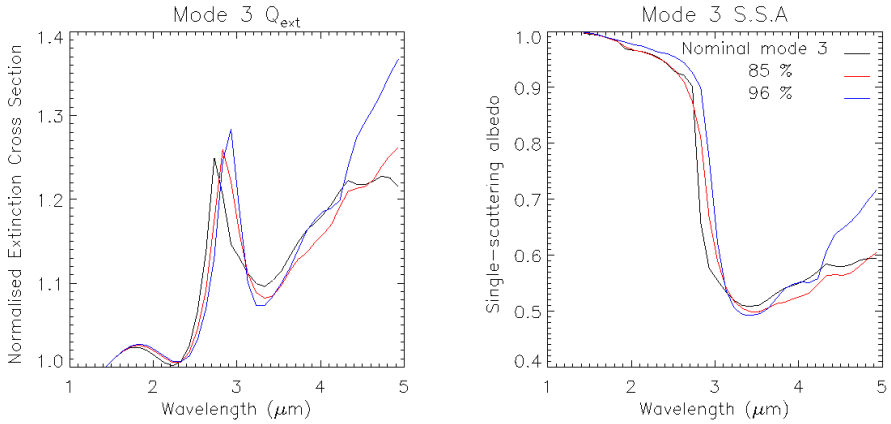

Figure 8: A comparison of extinction cross-section and single-scattering albedo generated for three different concentrations for mode 3 particles. Slight differences in the region of interest (2.3–2.5 μm) have little effect on the model spectra produced.

This process in fact reduced the goodness of fit for high cloud amount, as increasing the modal size of the particles decreased the single-scattering albedo and resulted in an increase in the absorptivity/emissivity (Figure 7).

6.3 Acid Concentration

The concentration of sulphuric acid in the cloud aerosols may be higher than the 75 wt % value used for the nominal Oxford cloud model, and in particular this may be different for the largest particles. Pollack et al. (1974) could not distinguish between a 75 wt % solution and a 95 wt % solution. Palmer & Williams (1975) also provide refractive index data for 85 and 96 wt % concentrations, so the effect of this on the mode 3 single-scattering albedo and extinction cross-section was investigated (Figure 8).

The effect of this was insufficient to produce the required improvement in the spectral shape, and in fact had little effect on the spectrum over the wavelength range of interest, meaning that any results obtained using this range are relatively insensitive to acid concentration.

6.4 Scale Height

The initial model test in Figure 5 was completed for a fractional scale height of 1.00 for all four cloud modes, meaning that the number density of cloud particles decreased with altitude at the same rate as the number density of gas molecules in the atmosphere. However, the cloud model of Crisp (1986) has a lower cloud absolute scale height approaching infinity – in other words, the number density in the lower cloud does not decrease noticeably with height. This is borne out by the results from the Pioneer Venus and Venera descent probe missions (Kliore et al. 1986).

Tests were initially completed with lower-cloud (modes 2' and 3) fractional scale heights of 3, 4 and 5, significantly increasing the absolute scale height from the initial model, from ∼6 km to ∼18—30 km. It can be seen immediately that there is an improvement in the model fit, particularly in the ratio of a bright spectrum to a dark spectrum, once the scale height is increased (Figure 9).

Once the scale height is increased to these values there is not a great deal of variation present in the quality of model fit, which is now much improved. A fractional scale heights of 4 produces the best quality of fit.

The other method of vertical redistribution of aerosols in the model is the alteration of the base altitude. Such alteration may be necessary to produce an optimal fit for both low- to mid-latitude and polar data, which display somewhat different bright:dark ratio shapes, indicating a different cloud regime polewards of 60°. This would be consistent with the findings of Wilson et al. (2008) and Titov et al. (2008).

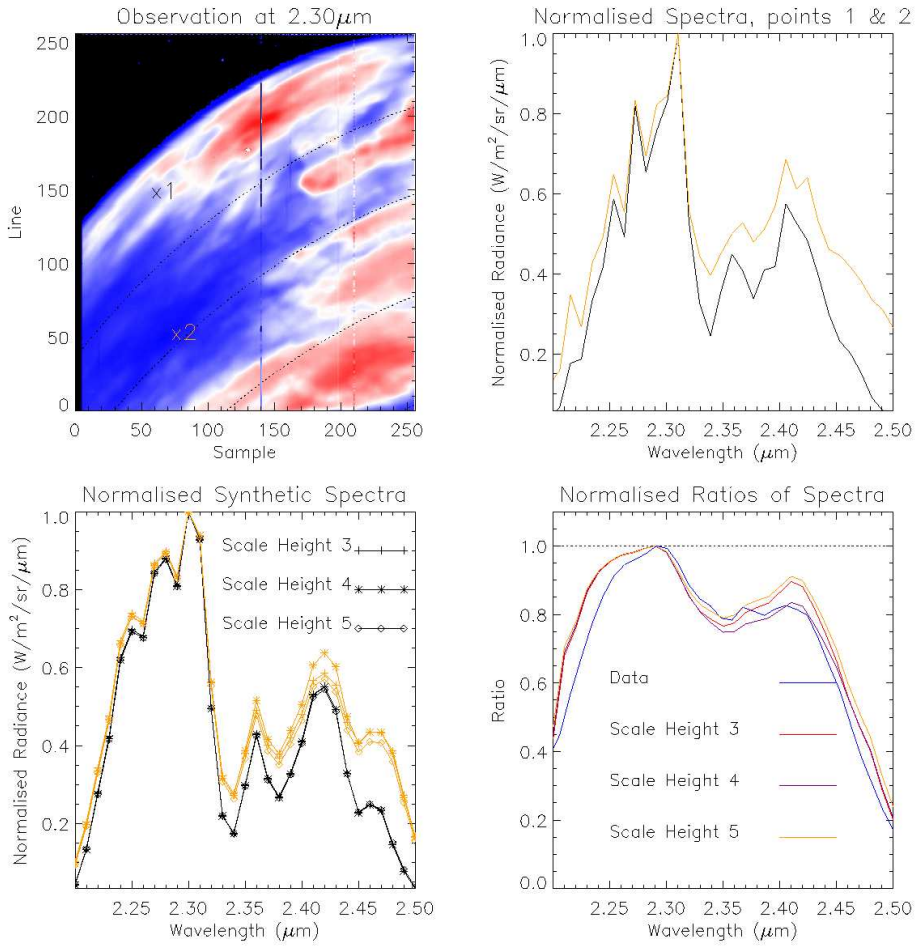

Figure 9: Model fits for lower-cloud fractional scale heights of 3–5. The base altitude is 45 km. The observation is VI0321_00, as above.

6.5 Base Altitude

A range of base altitudes from 43–52 km was investigated to find the best fit solution. A solution was viable for low- to mid-latitude data, using a fractional scale height of 4 and a nominal base altitude of 45 km. However, this was not straightforward for the polar data. It is likely that a failure so far to take into account possible variations in the average particle size at the poles is responsible (Wilson et al. 2008). Further progress must be made before a reliable a priori polar cloud model can be defined.

A small discrepancy at 2.4 μm between the model and data persists, even for the best fit case. This is particularly noticeable for the bright:dark spectral ratio. This work on the cloud model has been utilised by Tsang et al. (2009, in preparation), where it is suggested that this discrepancy is

due to a variation in water vapour abundance at ∼35 km that is negatively correlated with the optical thickness of the cloud. If a decreasing water vapour abundance with increasing cloud optical depth is introduced into the models, then for several spectra of varying radiances the model can be made to fit the data very well.

7 Mesoscale Variations in the Venus Cloud

7.1 The 2.54 μm Window

We observe a small radiance peak just longwards of the 2.3 μm window complex (shown in Figure 10), lying between 2.50 and 2.58 μm. It is reproduced by our forward model, but its strength appears to be variable in the VIRTIS data for spectra with the same 2.3 μm peak radiance. Because the radiance for this peak is ∼1 order of magnitude smaller than the 2.3 μm peak radiance, it can be difficult to distinguish from the noise, which is of order $10^(-3)$ W/m^2/sr/μm, so the observations used to investigate this window region are 24 observations each with an 18 s exposure time.

Because the strength of this window is observed to vary, it provides the opportunity to constrain a new mode of variability. In particular, variation in the ratio between the radiances at 2.3 and 2.53 μm can be mimicked by model spectra with different base altitudes. This window may therefore provide a constraint on the base altitude, and the observed variation may indicate that the base altitude is not constant, despite good agreement between the values of ∼46—48 km from the different descent probe datasets (Kliore et al. 1986).

Before this property can be investigated, sensitivity tests are necessary to determine which gaseous constituents, if any, the window is sensitive to. The temperature weighting function will also be a useful indication of the altitude sensitivity between 2.5 and 2.6 μm.

7.2 Sensitivity Tests

When a retrieval is performed using the *Nemesis* retrieval code, the functional derivatives of the model parameter(s) of interest are calculated as well as the forward model radiances for the current values of these parameters. This is also the case for a single forward model run if the parameter in question is included in the a priori file. If the given a priori for the parameter of interest is a continuous profile with height, then the derivative is calculated for each altitude level in the model and for each wavelength interval.

Functional derivatives of temperature are a useful indicator of the altitude sensitivity at any given wavelength. The temperature functional derivative, normalised in each wavelength bin, is shown in Figure 11.

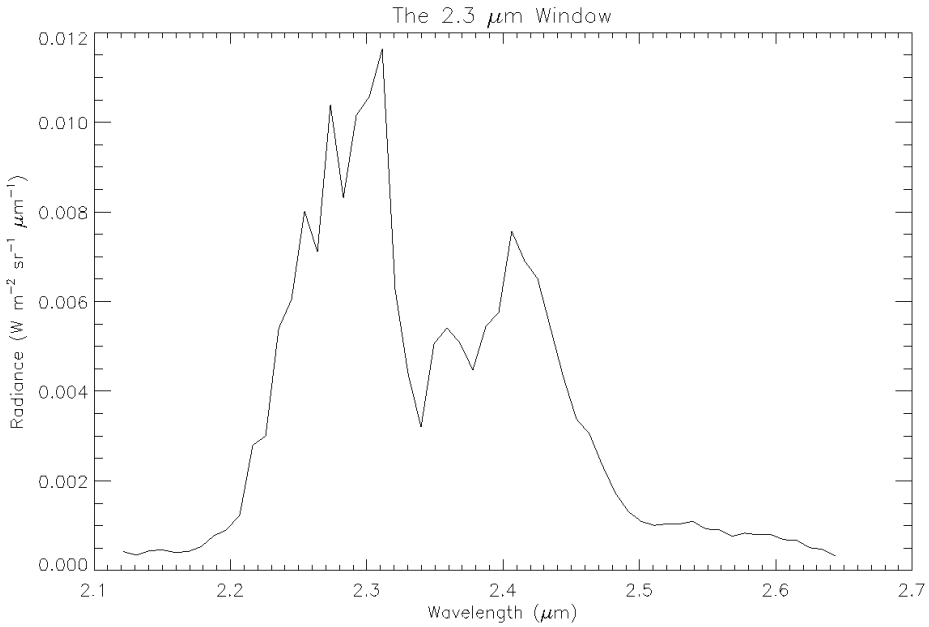

Figure 10: The 2.3 μm window. The sensitivities of the small shoulder between 2.5 and 2.6 μm have not been investigated prior to this work. This image is a spectrum from the VIRTISM-IR observation 0319_00.

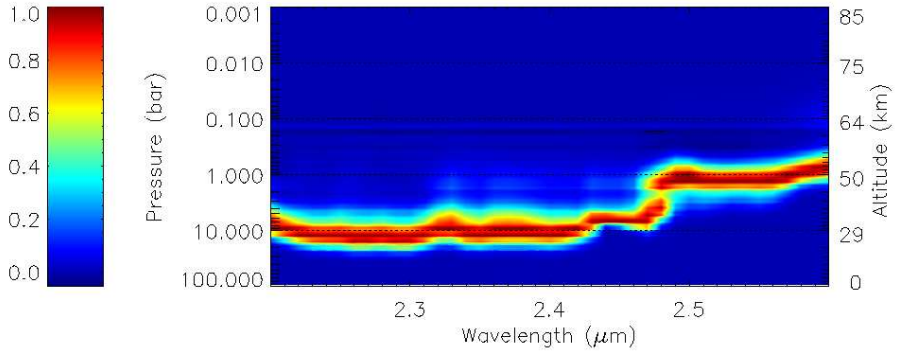

Figure 11: The sensitivity of an Oxford forward model spectrum to changes in temperature, with wavelength and altitude. Note that the altitude of maximum sensitivity is higher between 2.5 and 2.6 μm, at about 50 km (within the lower cloud layer).

This figure shows that the 2.5–2.6 μm region is sensitive at an altitude that we believe lies within the lower cloud. Sensitivity to cloud base altitude in this region is therefore likely. It is also possible that sensitivity to minor gaseous constituents at this altitude will allow further constraints on the vertical profiles of these constituents.

Sensitivity to the gases CO, H_2O, CH_4, OCS, SO_2, HF, HCl and H_2S has been tested in the region of interest, and the only one of these with a significant enough contribution for observation with VIRTIS-M to be a realistic prospect is H_2O. This is interesting, considering the potential of the 35 km altitude H_2O variation found by Tsang et al. (2009, in preparation) for providing constraints on dynamics and cloud formation processes. An example set of three forward models in the region of interest for three different scalings of the H_2O a priori vertical profile is shown in Figure 12.

However, cloud parameters also have an effect on this small window region. Clearly there is sensitivity to the total cloud optical depth, as in the other window regions, but from Figure 13 we also see that this region is sensitive to cloud base altitude. At the resolution of VIRTIS-M, the effect of water is not distinguishable from the effect of base altitude in this wavelength region alone. As the effect of base altitude is a grey effect across this wavelength range it may be possible to use VIRTIS-H to distinguish between this and water vapour, although the low signal-to-noise ratio is likely to be problematic. The base altitude is taken to be the base altitude for mode 2', which is the main contributor to opacity in the lower cloud.

7.3 The Branching Plot Method

In order to distinguish between the effects of water vapour and cloud base altitude with VIRTIS-M data, it is necessary to use a wider wavelength range than just the small window between 2.5 and 2.6 μm. The region between 2.3 and 2.5 μm is sensitive to the abundance of water vapour at $\sim$40 km, and if we assume that the a priori vertical distribution of water vapour that we are using represents the real vertical profile well we could in theory use a comparison between this region and the 2.5–2.6 μm region to simultaneously constrain both water vapour and cloud base altitude. Clearly, the assumption that the a priori vertical distribution is valid may be flawed, and this possibility must be investigated further, but for the following work I have considered the assumption to be valid.

One method that has been used previously to identify modes of variability in the data is the branching plot method. A branching plot is simply a plot of radiances for one wavelength against another for all the data points in a single observation. Deviations from a single branch indicate a variable quantity that produces a different response at the two different wavelengths. This method has been used by Carlson et al. (1993) and Wilson et al. (2008) to investigate alterations in the average size of cloud particles.

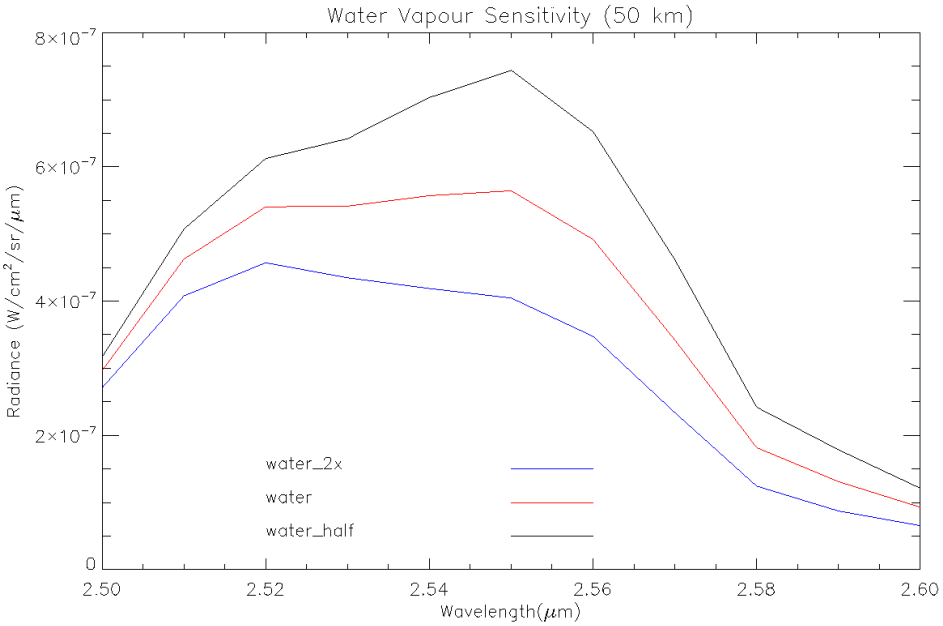

Figure 12: The effect on the forward model of multiplying the nominal water vapour profile by factors of a 0.5 and 2.0. The presence of a water band at $\sim$2.55 μm is indicated.

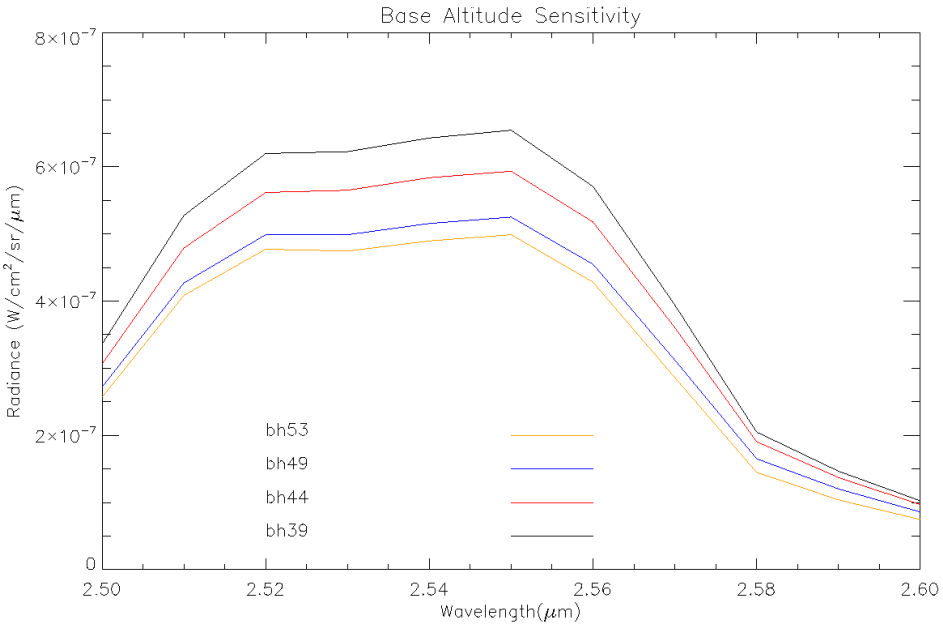

Figure 13: The effect on the forward model of varying the cloud base altitude. The sensitivity drops for a base altitude above $\sim$51 km.

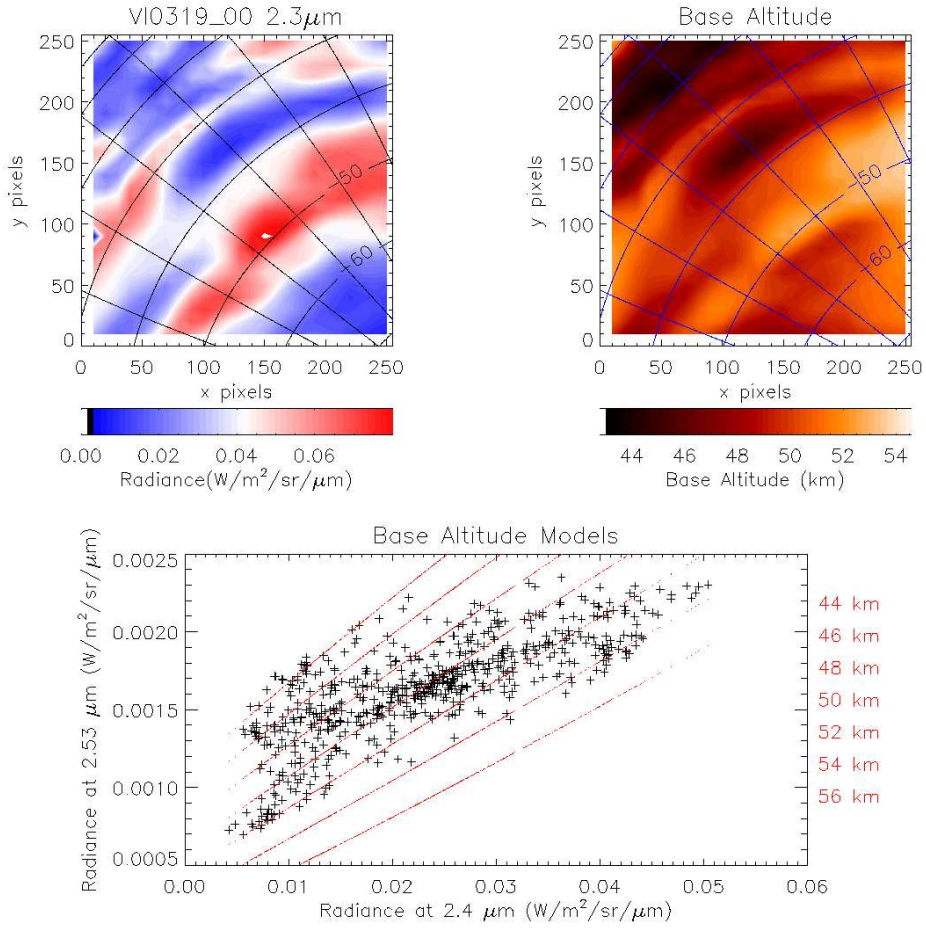

Figure 14: The inferred variation in base altitude from a branching plot of 2.53 v. 2.4 μm peak radiance for the observation 0319_00. Correlation can be seen between the base altitude and the 2.3 μm peak radiance. The red lines on the branch plot are second-order polynomial functions, extrapolated from polynomial fits to forward models created by *Nemesis*.

A branching plot of peak radiances at 2.53 μm versus peak radiances at 2.4 μm for a single observation has the useful property of being insensitive to variations in the abundance of water vapour, whilst showing strong variability with changes in base altitude. Forward models with different base altitudes and optical depths for mode 2' were generated, based on departures from the low- to mid-latitude a priori cloud described in Section 6. These models produce branches for different base altitudes that correspond well to branches observed in the data, and they can be fit by a second-order polynomial function. This property can then be used to produce quick 'model' branches and calculate an approximate value for base altitude for each data

point in a branching plot. An example result for this method is shown in Figure 14. It can be seen that there is definite correlation between the radiance at 2.3 μm and the base altitude, which corresponds to an anti-correlation between base altitude and cloud optical depth. The correlation coefficient R^2 obtained for VI0319_00 is 0.44.

7.4 Retrievals

Whilst the branching plot method is a good first indication that there is some variability in cloud base altitude and that it is related to the total cloud opacity, the method fails to take into account possible variations in CO and OCS abundances, which would alter the radiance at 2.4 μm. Therefore, to validate this method it is necessary to use *Nemesis* and perform a full retrieval.

I created a new parameterisation to enable *Nemesis* to retrieve the base altitude of a single cloud mode for a fixed total optical depth. This allowed me to perform a two-stage retrieval: stage one retrieves the relative optical depth of mode 2' with respect to the a priori optical depth using the wavelength range 2.15–2.3 μm, and stage two retrieves the relative abundances of CO, H_2O and OCS, and the base altitude, using the range 2.3–2.6 μm. Tests with synthetic noisy spectra confirmed the retrievability of these parameters, although the sensitivity to base altitude drops once it has increased beyond about 52 km.

In order to perform a retrieval on VIRTIS data, it is important to ensure that the signal-to-noise ratio is sufficiently high (at least 100) and also that there is no wavelength offset between the model and data. In order to achieve sufficient signal-to-noise, a coadding routine is used to average over squares of 20×20 pixels at intervals of 10 pixels in the 256×256 pixel spatial dimension of a VIRTIS data cube. Ignoring dark pixels and any squares for which the signal-to-noise falls below 100, this results in a 25×25 pixel image for each wavelength bin over the desired spectral range. The noise for each wavelength bin is calculated as follows:

$$N = N_i / \sqrt{t_{int} n_{pix}}, \tag{20}$$

where N is the calculated noise, N_i is the instrument noise, t_{int} is the integration time and n_{pix} is the number of coadded pixels.

VIRTIS-M has some variation in spectral registration across an image and has a wavelength offset of $\sim$+0.008 μm, so the coadding routine also cross-correlates the spectrum for each pixel against a normalised synthetic spectrum to remove the wavelength shift before the spectra are coadded.

The retrieval process is ongoing as the input forward modelling errors and a priori errors must be carefully chosen to optimise the goodness of fit, as indicated by the reduced χ^2 value output by *Nemesis*. This involves a significant amount of trial and error, and as the computing time for one observation is of the order of four days final results will take some time to complete. However, initial indications from these retrievals are that the base altitude variation indicated by the branch plot method does exist (Figure 15). The negative correlation between water vapour abundance and relative cloud opacity as reported by Tsang et al. (2009, in preparation) is observed, but there is also apparent correlation between areas of very thick cloud and

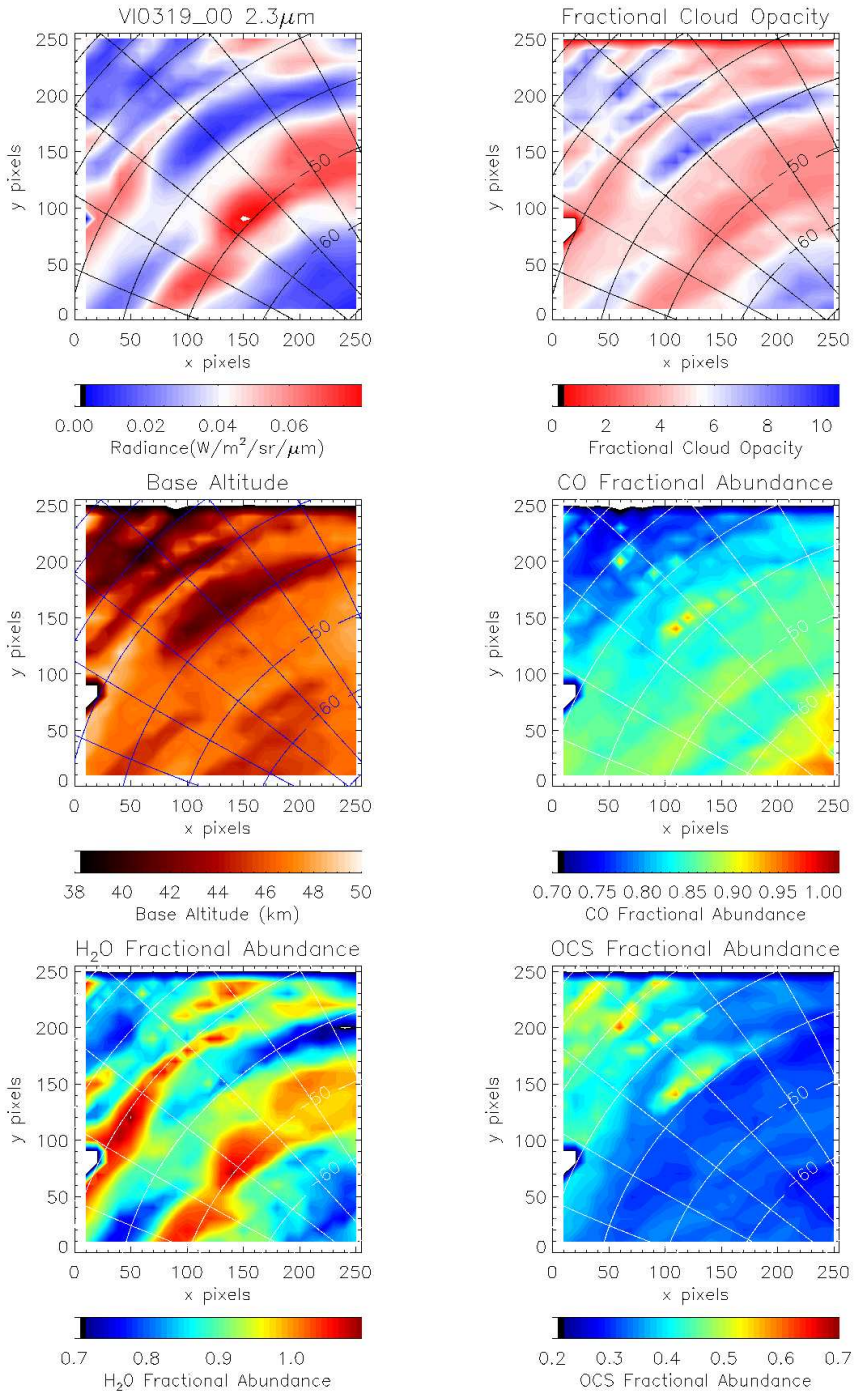

Figure 15: The 2.3 μm radiance for observation 0319_00 and retrieved relative cloud opacity, base altitude and relative gaseous abundances.

areas of high relative gaseous abundances. This may be caused by a failure of *Nemesis* to produce a good fit in areas of thick cloud, which of course have lower radiance spectra, but if these areas are still present with sufficiently low errors and off-diagonal correlation coefficients in the covariance matrix that are sufficiently close to zero then it may be a real effect.

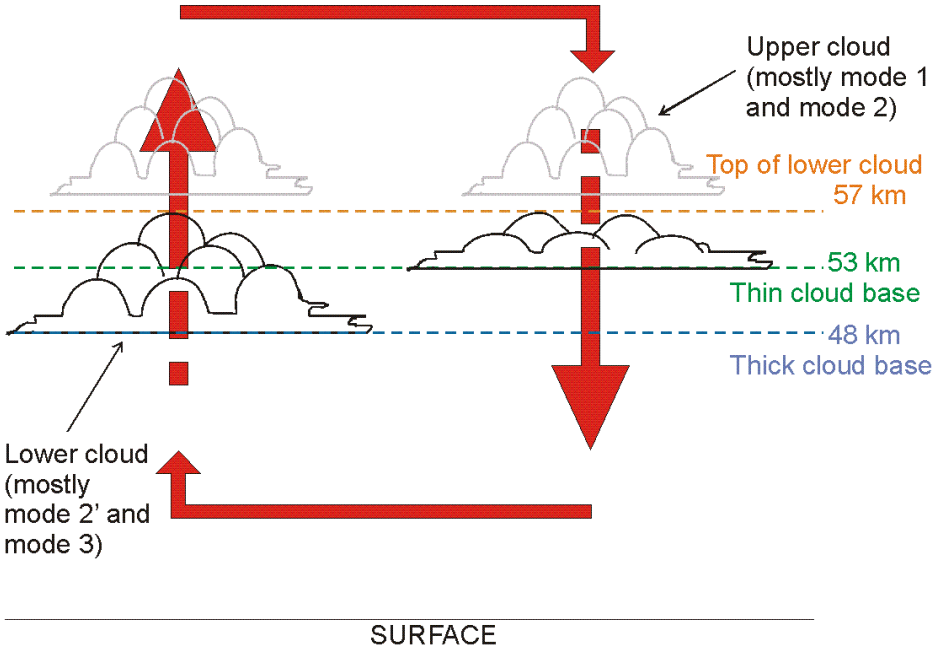

Figure 16: A simple representation of how cloud base variations may occur on Venus. Arrows indicate the presence of a convection cell. Thick cloud forms in regions of upwelling as H_2SO_4 vapour is transported upwards and condenses.

7.5 Possible Mechanisms

A possible model for cloud formation has been shown in Figure 4. Figure 16 shows how mesoscale convection may lead to differences in base altitude that correlate to the cloud opacity. Support for this theory may be found in the McGouldrick et al. (2008) paper on observations of cloud evolution, in which they postulate that the formation of holes in the cloud is related to convection on the scale observed here.

If the correlation between thick cloud and high gaseous abundances is confirmed, this could be the caused by active volcanism on Venus. All the gases retrieved here are constituents of volcanic gas, and we might expect an increase in SO_2 from volcanic outgassing to result in an increased level of cloud opacity. However, these measurements lie within the current error bars so further work on the retrieval process is needed before these results can be considered significant.

8 Plan for Future Work

8.1 Summary

The topic I have chosen for my thesis is the further study of the clouds of Venus. Several features of the cloud are poorly constrained and poorly understood, and as the cloud plays a significant role in the radiative balance of Venus it is a key area for study. An improved understanding of the cloud enables the creation of models which better represent the current atmosphere of Venus, and may also lead to an improved understanding of the coupling of the clouds with the other atmospheric constituents, dynamics and geology of Venus. A new cloud parameterisation would therefore have implications not just for radiative transfer modelling of Venus but also for dynamical modelling, microphysical cloud modelling, studies of volcanism and evolutionary modelling. The main goals of this research are to:

1. Implement a new cloud parameterisation that best represents the meridional and vertical distribution of the cloud, based on data from the VIRTIS instrument, and relate this if possible to global-scale dynamics.

2. Examine mesoscale departures from the above distribution and look for relationships with similar variations in gaseous abundances.

3. Investigate the possibility of observing the effects of volcanic outgassing on the formation of cloud.

8.1.1 Cloud Parameterisation

I intend to develop the work already completed on the low- to mid-latitude cloud model by examining the effects on this model of compositional/size differences in the cloud particles, using the *RADTRANS* code to generate forward models for comparison with VIRTIS spectra. I will endeavour to develop a similar parameterisation for the polar regions. I intend to make use of a large fraction of the VIRTIS spectral range to do this, particularly focusing on the windows at 1.74 and 2.3 μm which we know to be highly sensitive to variations in the cloud. I will also introduce a sub-micron haze below the clouds as postulated by Satoh et al. (2009) into our model to examine the effect.

My initial method, which I used in the development of the low- to mid-latitude cloud model, will be to look at the ratio of dark and bright spectra over the 2.3 μm window and attempt to reproduce this with forward models of similar peak radiances. I will then examine the effect of varying particle mode sizes, including the 1.74 μm window, as it has been postulated (Carlson et al. 1993, Wilson et al. 2008, Erard et al. 2009) that the average particle size changes in the polar regions.

I hope to finally have a reliable cloud model that provides a good representation of the planet-wide cloud structure, such that I can relate it to the dynamics and in particular the meridional Hadley cell transport.

8.1.2 Cloud Variation

Once a general model is in place, I will further develop my work examining base altitude variations across a single observation. A new base altitude retrieval parameterisation written for the *Nemesis* retrieval tool has already been implemented with some success, and I hope to extend this analysis to the polar regions and also to the sub-cloud haze. Radiative transfer modelling and retrievals on these scales would be complimentary to the microphysical modelling of such variations (McGouldrick & Toon 2007, McGouldrick et al. 2008, McGouldrick & Toon 2008). As it is possible to co-retrieve up to four parameters in a single run with *Nemesis*, abundances of gases can retrieved simultaneously with cloud parameters if the spectral region used is sensitive to them. This provides the opportunity to look for similarities in plots of cloud base altitude and plots of gaseous abundances, which may provide insight into mesoscale dynamics and cloud formation on these scales. At the time of writing a general model for low- to mid- latitudes is largely complete, and even if such a general model is not achievable in polar regions comparisons with the low-latitude model will facilitate further investigation.

8.1.3 Volcanism

Whilst detection of active volcanism may be possible through the identification of temperature anomalies, it is expected that a new crust would form rapidly over any volcanic outflow on Venus, leading to very short-lived hotspots, and therefore "the most sensitive detection could come from subtle variations in atmospheric composition above volcanic plumes or geysers" (Drossart et al. 2007). Water vapour and SO_2 are two of the major components of volcanic gas, and these gases react in the upper atmosphere of Venus to form sulphuric acid aerosol. Therefore, it might be expected that changes in the level of volcanic activity on Venus would affect the cloud opacity across the planet, and local activity may also affect the cloud locally. Variations in the abundance of SO_2 have been observed (Esposito et al. 1988), but so far have not been accepted as conclusive evidence for current volcanic activity. Anomalously high amounts of sulphuric acid aerosol may, as on Earth, be linked to volcanic activity (Baran et al. 1993), and this would be likely to have an impact on cloud opacity over timescales of a few months. Observations of such alterations in cloud opacity may be possible with VIRTIS data, and this may provide new evidence for volcanic activity on Venus. I will also compare any such anomalies with SPICAV/SOIR SO_2 abundance

measurements from the same period, if obtainable, although a direct comparison may be difficult as SPICAV/SOIR (Bertaux et al. 2007) SO_2 data are for regions above the cloud. Anomalously high values for CO and OCS may also be indicative of volcanic activity.

8.2 Timeline

An approximate timeline is included in the list below, with a Gantt chart in Figure 17:

January 09–December 09

1. To refine the current best-estimate low- to mid-latitude model.
2. To create a new polar cloud model.
3. To continue the base altitude retrievals for the low- to mid-latitude, 18-second exposure time VIRTIS-M observations.

January 10–May 10

1. To use the new polar cloud model to perform retrievals of base altitude and gaseous abundances at the poles.
2. To create and implement a general cloud model which takes into account changes in structure with latitude.
3. To look for variations from this general model on local scales.
4. To look for correlation between such variation and variation of gaseous abundances.
5. To investigate the sensitivity of the model to changes in cloud particle composition and size.

June 10–October 10

1. To investigate the effect of adding a sub-cloud haze to the radiative transfer model.
2. To implement a parameterisation for the retrieval of sub-cloud haze.
3. To look for correlation between any observed spatial variations in the sub-cloud haze and spatial variations within the main cloud deck.

November 10–March 11

1. To look for variations in cloud opacity and compare with SO_2 abundance variations, which may be indications of active volcanism.
2. To examine possible microphysical and dynamical mechanisms for any phenomena discovered above, possibly with GCM comparisons.

April 11–September 11

1. To make any necessary further refinements to the model.
2. To write up the work. I aim to have completed a study of Venusian cloud composition, vertical distribution and interaction on both global and smaller scales.

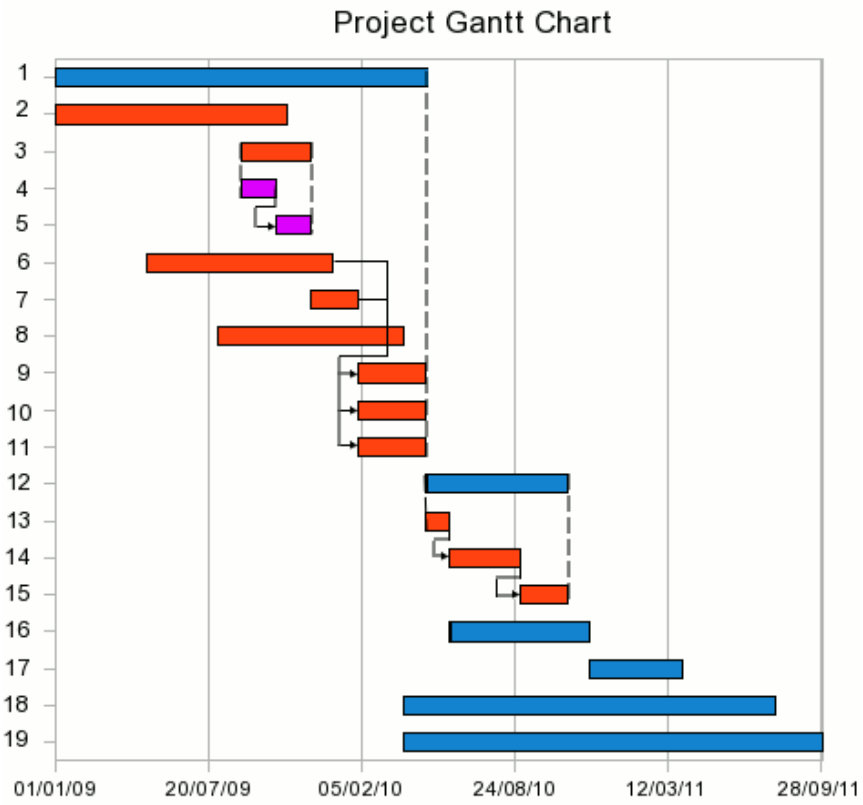

Task	Number
Investigating the vertical/spatial variability of the Venus clouds	1
Refine low-/mid-latitude cloud model	2
Create polar cloud model	3
Radiance ratio fit	4
Investigate effect of varying particle mode sizes	5
Base altitude/gas retrieval – low- & mid-latitude	6
Base altitude/gas retrieval – poles	7
Compare cloud structure with H2O/SO2 abundances	8
Compare with cloud-top data	9
Map latitudinal variation of cloud	10
Investigation of cloud compositional effects	11
Investigation of sub-cloud haze	12
Test sensitivity of the model to adding sub-cloud haze	13
Retrieve sub-cloud haze amount	14
Comparison with base altitude results	15
Cloud/volcanism search	16
Mechanisms for observed correlations	17
Refinements to the model	18
Write-up	19

Figure 17: A Gantt chart representation of my thesis plan. Colours refer to the hierarchy of tasks (purple→red→blue).

References

Allen, D. A. & Crawford, J. W. (1984), 'Cloud Structure on the Dark Side of Venus', *Nature* **307**, 222–224.

Baran, A. J., Foot, J. S. & Dibben, P. C. (1993), 'Satellite detection of volcanic sulphuric acid aerosol', *Geophysical Research Letters* **20**, 1799–1801.

Bertaux, J.-L., Nevejans, D., Korablev, O., Villard, E., Quémerais, E., Neefs, E., Montmessin, F., Leblanc, F., Dubois, J. P., Dimarellis, E., Hauchecorne, A., Lefèvre, F., Rannou, P., Chaufray, J. Y., Cabane, M., Cernogora, G., Souchon, G., Semelin, F., Reberac, A., van Ransbeek, E., Berkenbosch, S., Clairquin, R., Muller, C., Forget, F., Hourdin, F., Talagrand, O., Rodin, A., Fedorova, A., Stepanov, A., Vinogradov, I., Kiselev, A., Kalinnikov, Y., Durry, G., Sandel, B., Stern, A. & Gérard, J. C. (2007), 'SPICAV on Venus Express: Three spectrometers to study the global structure and composition of the Venus atmosphere', *Planetary and Space Science* **55**, 1673–1700.

Bullock, M. A. (1997), The Stability of Climate on Venus, PhD thesis, University of Colorado, Boulder, Colorado.

Bullock, M. A. & Grinspoon, D. H. (2001), 'The Recent Evolution of Climate on Venus', *Icarus* **150**, 19–37.

Carlson, R. W., Kamp, L. W., Baines, K. H., Pollack, J. B., Grinspoon, D. H., Encrenaz, T., Drossart, P. & Taylor, F. W. (1993), 'Variations in Venus cloud particle properties: A new view of Venus's cloud morphology as observed by Galileo Near-Infrared Mapping Spectrometer', *Planetary and Space Science* **41**, 477–485.

Cimino, J. (1982), 'The composition and vertical structure of the lower cloud deck on Venus', *Icarus* **51**, 334–357.

Colin, L. (1980), 'The Pioneer Venus Program', *Journal of Geophysical Research* **85**, 7575–7598.

Coradini, A., Capaccioni, F., Drossart, P., Semery, A., Arnold, G. & Schade, U. (1999), 'VIRTIS: The imaging spectrometer of the Rosetta mission', *Advances in Space Research* **24**, 1095–1104.

Coradini, A., Capaccioni, F., Drossart, P., Semery, A., Arnold, G., Schade, U., Angrilli, F., Barucci, M. A., Bellucci, G., Bianchini, G., Bibring, J. P., Blanco, A., Blecka, M., Bockelee-Morvan, D., Bonsignori, R., Bouye, M., Bussoletti, E., Capria, M. T., Carlson, R., Carsenty, U., Cerroni, P., Colangeli, L., Combes, M., Combi, M., Crovisier, J., Dami,

M., DeSanctis, M. C., DiLellis, A. M., Dotto, E., Encrenaz, T., Epifani, E., Erard, S., Espinasse, S., Fave, A., Federico, C., Fink, U., Fonti, S., Formisano, V., Hello, Y., Hirsch, H., Huntzinger, G., Knoll, R., Kouach, D., Ip, W. H., Irwin, P., Kachlicki, J., Langevin, Y., Magni, G., McCord, T., Mennella, V., Michaelis, H., Mondello, G., Mottola, S., Neukum, G., Orofino, V., Orosei, R., Palumbo, P., Peter, G., Pforte, B., Piccioni, G., Reess, J. M., Ress, E., Saggin, B., Schmitt, B., Stefanovitch, Stern, A., Taylor, F., Tiphene, D. & Tozzi, G. (1998), 'Virtis : an imaging spectrometer for the rosetta mission', *Planetary and Space Science* **46**, 1291–1304.

Crisp, D. (1986), 'Radiative forcing of the Venus mesosphere. I - Solar fluxes and heating rates', *Icarus* **67**, 484–514.

Donahue, T. M. (1979), 'Pioneer Venus results - an overview', *Science* **205**, 41–44.

Donahue, T. M., Hoffman, J. H., Hodges, R. R. & Watson, A. J. (1982), 'Venus was wet - A measurement of the ratio of deuterium to hydrogen', *Science* **216**, 630–633.

Drossart, P., Piccioni, G., Adriani, A., Angrilli, F., Arnold, G., Baines, K. H., Bellucci, G., Benkhoff, J., Bézard, B., Bibring, J.-P., Blanco, A., Blecka, M. I., Carlson, R. W., Coradini, A., di Lellis, A., Encrenaz, T., Erard, S., Fonti, S., Formisano, V., Fouchet, T., Garcia, R., Haus, R., Helbert, J., Ignatiev, N. I., Irwin, P. G. J., Langevin, Y., Lebonnois, S., Lopez-Valverde, M. A., Luz, D., Marinangeli, L., Orofino, V., Rodin, A. V., Roos-Serote, M. C., Saggin, B., Sanchez-Lavega, A., Stam, D. M., Taylor, F. W., Titov, D., Visconti, G., Zambelli, M., Hueso, R., Tsang, C. C. C., Wilson, C. F. & Afanasenko, T. Z. (2007), 'Scientific goals for the observation of Venus by VIRTIS on ESA/Venus express mission', *Planetary and Space Science* **55**, 1653–1672.

Erard, S., Drossart, P. & Piccioni, G. (2009), 'Multivariate analysis of Visible and Infrared Thermal Imaging Spectrometer (VIRTIS) Venus Express nightside and limb observations', *Journal of Geophysical Research (Planets)* **114**(E13).

Esposito, L. W., Copley, M., Eckert, R., Gates, L., Stewart, A. I. F. & Worden, H. (1988), 'Sulfur dioxide at the Venus cloud tops, 1978-1986', *Journal of Geophysical Research* **93**, 5267–5276.

Esposito, L. W., Knollenberg, R. G., Marov, M. I., Toon, O. B. & Turco, R. P. (1983), *The clouds and hazes of Venus*, The University of Arizona, pp. 484–564.

Grinspoon, D. H., Pollack, J. B., Sitton, B. R., Carlson, R. W., Kamp, L. W., Baines, K. H., Encrenaz, T. & Taylor, F. W. (1993), 'Probing Venus's cloud structure with Galileo NIMS', *Planetary and Space Science* **41**, 515–542.

Hashimoto, G. L. & Abe, Y. (2005), 'Climate control on Venus: Comparison of the carbonate and pyrite models', *Planetary and Space Science* **53**, 839–848.

Head, III, J. W., Crumpler, L. S. & Aubele, J. C. (1992), 'Venus volcanism: A global overview from Magellan data', *LPI Contributions* **789**, 43–45.

Helbert, J., Müller, N., Kostama, P., Marinangeli, L., Piccioni, G. & Drossart, P. (2008), 'Surface brightness variations seen by VIRTIS on Venus Express and implications for the evolution of the Lada Terra region, Venus', *Geophysical Research Letters* **35**.

Henyey, L. G. & Greenstein, J. L. (1941), 'Diffuse radiation in the Galaxy', *Astrophysical Journal* **93**, 70–83.

Houze, Jr., R. A. (1993), *Cloud Dynamics*, Academic Press.

Imamura, T. & Hashimoto, G. L. (2002), 'H_2SO_4 cycle in the Venusian tropical atmosphere as constrained by a microphysical cloud model', *Advances in Space Research* **29**, 249–254.

Irwin, P. G. J., Calcutt, S. B. & Taylor, F. W. (1997), 'Radiative transfer models for Galileo NIMS studies of the atmosphere of Jupiter', *Advances in Space Research* **19**, 1149–1158.

Irwin, P. G. J., Teanby, N. A., de Kok, R., Fletcher, L. N., Howett, C. J. A., Tsang, C. C. C., Wilson, C. F., Calcutt, S. B., Nixon, C. A. & Parrish, P. D. (2008), 'The NEMESIS planetary atmosphere radiative transfer and retrieval tool', *Journal of Quantitative Spectroscopy and Radiative Transfer* **109**, 1136–1150.

Kamp, L. W. & Taylor, F. W. (1990), 'Radiative-transfer models of the night side of Venus', *Icarus* **86**, 510–529.

Kliore, A., Moroz, V. & G., K. (1986), *The Venus International Reference Atmosphere*, Pergamon Press, Oxford.

Knollenberg, R. G. & Hunten, D. M. (1980), 'The microphysics of the clouds of Venus - Results of the Pioneer Venus particle size spectrometer experiment', *Journal of Geophysical Research* **85**, 8039–8058.

Kolodner, M. A. & Steffes, P. G. (1998), 'The Microwave Absorption and Abundance of Sulfuric Acid Vapor in the Venus Atmosphere Based on New Laboratory Measurements', *Icarus* **132**, 151–169.

Lacis, A. A. & Oinas, V. (1991), 'A description of the correlated-k distribution method for modelling nongray gaseous absorption, thermal emission, and multiple scattering in vertically inhomogeneous atmospheres', *Journal of Geophysical Research* **96**, 9027–9064.

Marcq, E., Bézard, B., Encrenaz, T. & Birlan, M. (2005), 'Latitudinal variations of CO and OCS in the lower atmosphere of Venus from near-infrared nightside spectro-imaging', *Icarus* **179**, 375–386.

Marov, M. Y. (1978), 'Results of Venus missions', *Annual Review of Astronomy and Astrophysics* **16**, 141–169.

McGouldrick, K., Baines, K. H., Momary, T. W. & Grinspoon, D. H. (2008), 'Venus Express/VIRTIS observations of middle and lower cloud variability and implications for dynamics', *Journal of Geophysical Research (Planets)* **113**(E12).

McGouldrick, K. & Toon, O. B. (2007), 'An investigation of possible causes of the holes in the condensational Venus cloud using a microphysical cloud model with a radiative-dynamical feedback', *Icarus* **191**, 1–24.

McGouldrick, K. & Toon, O. B. (2008), 'Observable effects of convection and gravity waves on the Venus condensational cloud', *Planetary and Space Science* **56**, 1112–1131.

Meadows, V. S. & Crisp, D. (1996), 'Ground-based near-infrared observations of the Venus nightside: The thermal structure and water abundance near the surface', *Journal of Geophysical Research* **101**, 4595–4622.

Myhre, C. E. L., Christensen, D. H., Nicolaisen, D. H. & Neilsen, C. J. (2003), 'Spectroscopic Study of Aqueous H_2SO_4 at Different Temperatures and Compositions: Variations in Dissociation and Optical Properties', *Journal of Physical Chemistry* **107**, 1979–1991.

Palmer, K. F. & Williams, D. (1975), 'Optical constants of sulfuric acid: application to the clouds of Venus?', *Applied Optics* **14**, 208–219.

Petropoulos, B. & Telonis, P. (1988), 'The lower atmosphere of Venus after VEGA 1 and 2 missions', *Earth Moon and Planets* **43**, 45–60.

Piccialli, A., Titov, D. V., Grassi, D., Khatuntsev, I., Drossart, P., Piccioni, G. & Migliorini, A. (2008), 'Cyclostrophic winds from the Visible and Infrared Thermal Imaging Spectrometer temperature sounding: A preliminary analysis', *Journal of Geophysical Research (Planets)* **113**(E12).

Piccioni, G., Drossart, P., Sanchez-Lavega, A., Hueso, R., Taylor, F. W., Wilson, C. F., Grassi, D., Zasova, L., Moriconi, M., Adriani, A., Lebonnois, S., Coradini, A., Bézard, B., Angrilli, F., Arnold, G., Baines, K. H., Bellucci, G., Benkhoff, J., Bibring, J. P., Blanco, A., Blecka, M. I., Carlson, R. W., di Lellis, A., Encrenaz, T., Erard, S., Fonti, S., Formisano, V., Fouchet, T., Garcia, R., Haus, R., Helbert, J., Ignatiev, N. I., Irwin, P. G. J., Langevin, Y., Lopez-Valverde, M. A., Luz, D., Marinangeli, L., Orofino, V., Rodin, A. V., Roos-Serote, M. C., Saggin, B., Stam, D. M., Titov, D., Visconti, G., Zambelli, M., Ammannito, E., Barbis, A., Berlin, R., Bettanini, C., Boccaccini, A., Bonnello, G., Bouye, M., Capaccioni, F., Cardesin Moinelo, A., Carraro, F., Cherubini, G., Cosi, M., Dami, M., de Nino, M., Del Vento, D., di Giampietro, M., Donati, A., Dupuis, O., Espinasse, S., Fabbri, A., Fave, A., Veltroni, I. F., Filacchione, G., Garceran, K., Ghomchi, Y., Giustini, M., Gondet, B., Hello, Y., Henry, F., Hofer, S., Huntzinger, G., Kachlicki, J., Knoll, R., Driss, K., Mazzoni, A., Melchiorri, R., Mondello, G., Monti, F., Neumann, C., Nuccilli, F., Parisot, J., Pasqui, C., Perferi, S., Peter, G., Piacentino, A., Pompei, C., Reess, J.-M., Rivet, J.-P., Romano, A., Russ, N., Santoni, M., Scarpelli, A., Semery, A., Soufflot, A., Stefanovitch, D., Suetta, E., Tarchi, F., Tonetti, N., Tosi, F. & Ulmer, B. (2007), 'South-polar features on Venus similar to those near the north pole', *Nature* **450**, 637–640.

Pollack, J. B., Erickson, E. F., Witteborn, F. C., Chackerian, Jr., C., Summers, A. L., van Camp, W., Baldwin, B. J., Augason, G. C. & Caroff, L. J. (1974), 'Aircraft observations of Venus' near-infrared reflection spectrum - Implications for cloud composition', *Icarus* **23**, 8–26.

Pollack, J., Dalton, J., Grinspoon, D., Wattson, R., Freedman, R., Crisp, D., Allen, D., Bézard, B., de Bergh, C. & Giver, L. (1993), 'Near-Infrared Light from Venus' Nightside: A Spectroscopic Analysis', *Icarus* **103**, 1–42.

Prinn, R. G. (1978), 'Venus - Chemistry of the lower atmosphere prior to the Pioneer Venus mission', *Geophysical Research Letters* **5**, 973–976.

Rodgers, C. D. (2000), *Inverse Methods for Atmospheric Sounding*, World Scientific.

Rogers, R. R. & Yau, M. K. (1989), *A Short Course in Cloud Physics*, third edn, Pergamon Press.

Rothman, L. S., Barbe, A., Benner, D. C., Brown, L. R., Camy-Peyret, C., Carleer, M. R., Chance, K., Clerbaux, C., Dana, V., Devi, V. M., Fayt, A., Flaud, J. M., Gamache, R. R., Goldman, A., Jacquemart, D.,

Jucks, K. W., Lafferty, W. J., Mandin, J. Y., Massie, S. T., Nemtchinov, V., Newnham, D. A., Perrin, A., Rinsland, C. P., Schroeder, J., Smith, K. M., Smith, M. A. H., Tang, K., Toth, R. A., Auwera, J. V., Varanasi, P. & Yoshino, K. (2003), 'The hitran molecular spectroscopic database: edition of 2000 including updates through 2001', *Journal of Quantitative Spectroscopy and Radiative Transfer* **82**(1-4), 5 – 44. The HITRAN Molecular Spectroscopic Database: Edition of 2000 Including Updates of 2001.

Rusk, A. N., Williams, D. & Querry, M. R. (1971), 'Optical Constants of Water in the Infrared', *Journal of the Optical Society of America* **61**, 895–903.

Sagan, C. (1960), 'The Surface Temperature of Venus.', *Astronomical Journal* **65**, 352–353.

Sagan, C. (1962), 'Structure of the lower atmosphere of Venus', *Icarus* **1**, 151–169.

Satoh, T., Imamura, T., Hashimoto, G. L., Iwagami, N., Mitsuyama, K., Sorahana, S., Drossart, P. & Piccioni, G. (2009), 'Cloud structure in Venus middle-to-lower atmosphere as inferred from VEX/VIRTIS 1.74 μm data', *Journal of Geophysical Research (Planets)* **114**(E13).

Saunders, R. S. & Malin, M. C. (1977), 'Geologic interpretation of new observations of the surface of Venus', *Geophysical Research Letters* **4**, 547–550.

Seiff, A., Schofield, J. T., Kliore, A. J., Taylor, F. W. & Limaye, S. S. (1985), 'Models of the structure of the atmosphere of Venus from the surface to 100 kilometers altitude', *Advances in Space Research* **5**, 3–58.

Svedhem, H., Titov, D. V., McCoy, D., Lebreton, J.-P., Barabash, S., Bertaux, J.-L., Drossart, P., Formisano, V., Häusler, B., Korablev, O., Markiewicz, W. J., Nevejans, D., Pätzold, M., Piccioni, G., Zhang, T. L., Taylor, F. W., Lellouch, E., Koschny, D., Witasse, O., Eggel, H., Warhaut, M., Accomazzo, A., Rodriguez-Canabal, J., Fabrega, J., Schirmann, T., Clochet, A. & Coradini, M. (2007), 'Venus Express—The first European mission to Venus', *Planetary and Space Science* **55**, 1636–1652.

Taylor, F. & Grinspoon, D. (2009), 'Climate evolution of Venus', *Journal of Geophysical Research (Planets)* **114**(E13).

Taylor, F. W., Diner, D. J., Elson, L. S., McCleese, D. J., Martonchik, J. V., Delderfield, J., Bradley, S. P., Schofield, J. T., Gille, J. C. & Coffey, M. T. (1979), 'Temperature, cloud structure, and dynamics of Venus

middle atmosphere by infrared remote sensing from Pioneer Orbiter', *Science* **205**, 65–67.

Teanby, N. A., de Kok, R., Irwin, P. G. J., Osprey, S., Vinatier, S., Gierasch, P. J., Read, P. L., Flasar, F. M., Conrath, B. J., Achterberg, R. K., Bézard, B., Nixon, C. A. & Calcutt, S. B. (2008), 'Titan's winter polar vortex structure revealed by chemical tracers', *Journal of Geophysical Research (Planets)* **113**(E12).

Titov, D. V., Svedhem, H., Koschny, D., Hoofs, R., Barabash, S., Bertaux, J.-L., Drossart, P., Formisano, V., Häusler, B., Korablev, O., Markiewicz, W. J., Nevejans, D., Pätzold, M., Piccioni, G., Zhang, T. L., Merritt, D., Witasse, O., Zender, J., Accomazzo, A., Sweeney, M., Trillard, D., Janvier, M. & Clochet, A. (2006), 'Venus Express science planning', *Planetary and Space Science* **54**, 1279–1297.

Titov, D. V., Taylor, F. W., Svedhem, H., Ignatiev, N. I., Markiewicz, W. J., Piccioni, G. & Drossart, P. (2008), 'Atmospheric structure and dynamics as the cause of ultraviolet markings in the clouds of Venus', *Nature* **456**, 620–623.

Tsang, C. C. C. (2007), The Composition and Circulation of the Atmosphere of Venus using Venus Express/VIRTIS Data, PhD thesis, Atmospheric, Oceanic and Planetary Physics, Department of Physics University of Oxford.

Tsang, C. C. C., Irwin, P. G. J., Wilson, C. F., Taylor, F. W., Lee, C., de Kok, R., Drossart, P., Piccioni, G., Bezard, B. & Calcutt, S. (2008b), 'Tropospheric carbon monoxide concentrations and variability on Venus from Venus Express/VIRTIS-M observations', *Journal of Geophysical Research (Planets)* **113**(E12).

Tsang, C. C. C., Wilson, C. F., Barstow, J. K., Bézard, B., Irwin, P. G. J., Taylor, F. W., Piccioni, G., Drossart, P., McGouldrick, K. & Calcutt, S. B. (2009, in preparation), 'Water vapour depletion in regions of optically thick cloud on Venus', *Nature* .

Tsang, C., Irwin, P., Taylor, F. & Wilson, C. (2008a), 'A correlated-k model of radiative transfer in the near-infrared windows of venus', *Journal of Quantitative Spectroscopy and Radiative Transfer* **109**(6), 1118 – 1135. Spectroscopy and Radiative Transfer in Planetary Atmospheres.

Tsang, C., Taylor, F., Wilson, C., Liddell, S., Irwin, P., Piccioni, G., Drossart, P. & Calcutt, S. (2009), 'Variability of co concentrations in the venus troposphere from venus express/virtis using a band ratio technique', *Icarus* **201**(2), 432 – 443.

Urey, H. C. (1952), *The Planets*, Yale University Press.

Wilson, C. F., Guerlet, S., Irwin, P. G. J., Tsang, C. C. C., Taylor, F. W., Carlson, R. W., Drossart, P. & Piccioni, G. (2008), 'Evidence for anomalous cloud particles at the poles of Venus', *Journal of Geophysical Research (Planets)* **113**(E12).

Young, A. T. (1973), 'Are the Clouds of Venus Sulfuric Acid?', *Icarus* **18**, 564–582.

Zhang, T. L., Baumjohann, W., Delva, M., Auster, H.-U., Balogh, A., Russell, C. T., Barabash, S., Balikhin, M., Berghofer, G., Biernat, H. K., Lammer, H., Lichtenegger, H., Magnes, W., Nakamura, R., Penz, T., Schwingenschuh, K., Vörös, Z., Zambelli, W., Fornacon, K.-H., Glassmeier, K.-H., Richter, I., Carr, C., Kudela, K., Shi, J. K., Zhao, H., Motschmann, U. & Lebreton, J.-P. (2006), 'Magnetic field investigation of the Venus plasma environment: Expected new results from Venus Express', *Planetary and Space Science* **54**, 1336–1343.